Peertechz

Life Sciences Group

International Journal of Nanomaterials, Nanotechnology and Nanomedicine

ISSN: 2455-3492 DOI CC By

M Benhamou[1]* and S El-Moudny[2]

[1]Physics Department, Faculty of Sciences, PO Box 11201, Moulay Ismail University, Meknes, Morocco
[2]ENSAM, Moulay Ismail University, PO Box 15290, Al Mansour, Meknes, Morocco

Dates: Received: 10 June, 2017; **Accepted:** 30 August, 2017; **Published:** 31 August, 2017

***Corresponding author:** M Benhamou, Physics Department, Faculty of Sciences, PO Box 11201, Moulay Ismail University, Meknes, Morocco, E-mail: m.benhamou@ensam-umi.ac.ma

Keywords: Pickering emulsions; Nanoparticles; Structure; Thermodynamics; Cage effect; Sub diffusion; Spherical diffusion

https://www.peertechz.com

Review Article

Review on Pickering emulsions stabilized by adsorbed nanoparticles: Structure, Thermodynamics, Cage Effect and Subdiffusion

Abstract

In this review paper, we report on some very recent findings dealt with the oil-in-water Pickering emulsions, stabilized by a strong adsorption of charged solid nanoparticles on the surface of the oil-droplets. Here, we are concerned with three important questions: (1) Structure and thermodynamics of these emulsions, (2) cage effect and subdiffusion phenomenon within them, and (3) spherical diffusion of anchored nanoparticles on the curved oil/water interface. For the study, the emulsions are regarded as colloidal solutions, where the clothed oil-droplets play the role of charged soft-colloids, and in addition, the adsorbed nanoparticles are assumed to be point-like. For question (1), we recall the essential steps allowing the determination of the structure-factor and the spatial-correlation function, and the thermodynamic properties, as pressure, internal energy, and thermal compressibility of these emulsions. To this end, the adopted pair-potential is that of Sogami-Ise combining repulsive and attractive forces, and use is made of the so-called *Integral Equation Method*. The question (2) deals with a quantitative investigation of the clothed oil-droplets dynamics (cage effect and subdiffusion), using a *Generalized Langevin Equation*, which is successfully tested by *Molecular Dynamic Simulations*. The question (3) is concerned with an *exact* study of the spherical diffusion of anchored nanoparticles on the surface of the dispersed oil-droplets. Finally, we precise the major role played by grafted polymers onto the spherical oil/water interface.

Introduction

Pickering emulsions (PEs) [1,2], are dispersions presenting, very often, as oil-in-water (O/W), water-in-oil (W/O) or double emulsion water-oil-water (W/O/W). These dispersions are stabilized by an addition of small solid particles that act as *emulsifiers*, instead of the surfactant molecules [3-6]. These particles may be organic or inorganic, according to the nature of their desired use. Also, PEs may be water-in-water (W/W) emulsions [7], which are dispersions formed by droplets of water-solvated molecules moving in another continuous aqueous solution. Both droplets and continuous phase contain different molecules (chemically incompatible macromolecules, for instance), which are entirely water-soluble. The solid particles that act as emulsifiers are of *nanometric* size, while the stabilized droplets are as small as few *micrometers* diameter. The stabilization of larger droplets (few millimeters diameter) is possible as well, using micron-sized solid particles.

The stabilization of the dispersed droplets within PEs is ensured by a strong adsorption of the solid particles at their surfaces. In contrary to surfactants, where the adsorption is rather dynamic (reversible), that of the charged solid particles is irreversible and sufficiently strong, with a very high adsorption energy, between $10^6 k_B T$ and $10^8 k_B T$, where $k_B T$ is the thermal energy. Here, k_B is the Boltzmann's constant and T is the bath temperature. Of course, such an energy mainly depends on the value of the wetting (or contact) angle and the droplet-radius [6]. The anchoring of the solid particles emanates from a partial wetting of the surface of the charged solid particles by water and oil.

Due to their remarkable properties, such as high stability with respect to coalescence and their recent use in nanotechnology leading to the creation and the characterization of the nano-scale structures in new ways, PEs have been the subject of much studies, both from experimental and theoretical point of views. In addition, they can serve as templates for the advanced materials, as Janus colloids [8], composite particles [9-18], and colloidosomes [19-21].

PEs are heterogenous liquids which present as a dispersion of droplets of some liquid (*dispersed phase*) in another one (*continuous phase*). A typical example is schematized in figure 1.

Citation: Benhamou M, El-Moudny S (2017) Review on Pickering emulsions stabilized by adsorbed nanoparticles: Structure, Thermodynamics, Cage Effect and Subdiffusion. Int J Nanomater Nanotechnol Nanomed 3(2): 057-076. DOI: http://doi.org/10.17352/2455-3492.000022

The two liquids are not chemically and physically compatible. By a mechanical mixing of the emulsion, each droplet becomes surrounded by discrete nanoparticles arranged on its surface. If the preparing conditions, such as wettability [22-30], charge [31-34], concentration [3], shape and size [35-40], of nanoparticles, as well as, the pH and the salt-concentration in aqueous phase [41-44], are right, the clothed droplets can be regarded as charged *soft-colloids* [45].

Beside their use in industry as special emulsions, PEs have other potential applications. In fact, they were recently used [46], for the preparation of the so-called magnetic polymer microspheres [47] (*magnetic balls*), which possess polymer cores that are protected by shells of magnetic nanoparticles, where oil is styrene, emulsified in an aqueous dispersion of Fe3O4-nanoparticles using a high shear. The oil-in-water emulsion is stabilized by magnetic nanoparticles, and styrene was easily polymerized at temperature 70°C. Iron oxide nanoparticles then act as effective stabilizers during the polymerization process. The fabricated magnetic nanocomposites were characterized using the standard experimental techniques.

Generally, the stabilization of PEs is ensured by the charge carried by the anchored nanoparticles. But the resulting Coulomb force between the (oil) hairy-droplets are screened out by the presence of mobile small charges that are counterions and coions (coming from a dissociation of an electrolyte). In a very recent publication [48], the authors were interested in the determination of the structure and thermodynamics of PEs, using the so-called *Integral Equation Method* [49], which is based on the Statistical Mechanics principles. Such a method allowed the extraction of the spatial-correlation-function and the structure-factor and thermodynamic properties, as pressure, internal energy and thermal compressibility. To approach the static problem, the authors first considered the clothed oil-droplets as monodisperse small spheres assimilated to charged *soft-colloids*. When the temperature of the considered emulsion is fixed to some value (room temperature), the only remaining parameters of discussion are the density of droplets, their size and surface charge, and the salt-concentration. For the study, the adopted pair-potential was of Sogami-Ise type [50,51], which is an alternative of the standard Derjaguin-Landau-Verwey-Overbeek (DLVO) potential [52]. Thereafter, the question [53] was addressed to investigate quantitatively the *cage effect* and the *subdiffusion phenomenon* within PEs. Such an anomalous diffusion originates from the fact that PEs are heterogenous (or complex) systems, where their constituents are strongly correlated. To this end, use was made of *Molecular Dynamics Simulations*. This computational method was introduced by Alder and Wainwright [54], in order to study the structure and dynamics of liquids. Also, an *exact* study of the spherical diffusion laws of anchored nanoparticles on the surface of the droplets of PEs has been recently achieved [55]. These exact spherical diffusion laws have been determined using the *Green's function* techniques (further details are given below).

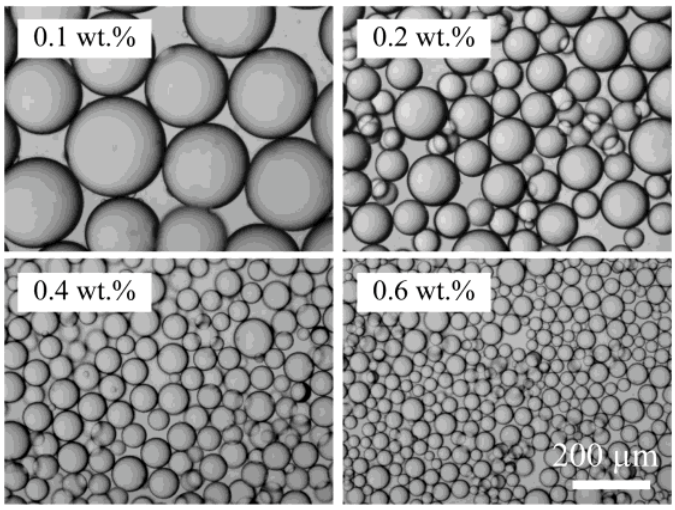

Figure 1: Optical microscopy images of O/W emulsions prepared at pH 4.7 stabilised by WPM particles of different concentration in water.

For some industrial purposes, the association of polymers to PEs is strongly recommended, in order to synthesize new nanocomposites dedicated to specific applications. Many experimental works have been devoted to such a question. For example, in a recent experimental paper [56], PEs were stabilized by cellulose monocrystals grafted with thermo-responsive polymer brushes. An another example is provided by some recent experiment [57], dealt with PEs stabilized by nanoparticles with thermally responsive grafted polymer brushes. In the same context, dual responsive PEs stabilized by constructed core crosslinked polymer nanoparticles via reversible covalent bonds are reported Ref. [58]. Another interesting work [59] was recently achieved to tunable PEs with polymer-grafted lignin nanoparticles. It is well-known that lignin is an abundant biopolymer that has native interfacial functions but aggregates strongly in aqueous media. In this experiment, the polyacrylamide was grafted onto kraft lignin nanoparticles, using reversible addition-fragmentation chain transfer chemistry to form polymer-grafted lignin nanoparticles. The study of PEs stabilized by palygorskite particles grafted with pH-responsive polymer brushes was the goal of a recent experimental investigation [60]. The one-step formation of multiple PEs stabilized by the self-assembled poly (dodecyl acrylate-co-acrylic acid) nanoparticles as emulsifiers has been the subject of some experimental work [61]. As last example, we recall that a new approach to the formation of cross-linked colloidosomes was developed [62], on the basis of PEs, stabilized exclusively by peroxidized colloidal particles.

When the nanoparticles that emulsify the dispersion, are electrically uncharged or neutral, the most effective way to stabilize PEs consists in grafting polymer chains onto the surface of the dispersed (oil or water) droplets. Before adding the polymer chains to the emulsion, one terminates each by a solid nanoparticle that has no particular preference for the two immiscible liquids. Then, the polymer chains associated to the solid nanoparticles, go to the oil/water interface to form hairy-droplets, where the chains float in the surrounding liquid. Also, use can be made of the polymer chains, which are terminated rather by big amphiphilic molecules (O/W case). Therefore, in this case, the grafted-polymer chains play the role of surfactants. Also, one can use *telechelic polymers* (di-

Citation: Benhamou M, El-Moudny S (2017) Review on Pickering emulsions stabilized by adsorbed nanoparticles: Structure, Thermodynamics, Cage Effect and Subdiffusion. Int J Nanomater Nanotechnol Nanomed 3(2): 057-076. DOI: http://doi.org/10.17352/2455-3492.000022

end-functional polymers) [63], or diblock polymers (one sequence prefers to contact water, and the other, oil) to get hairy-droplets. In a recent study [64], the aim was a *rigorous* theoretical determination of the expression of the effective potential between hairy-droplets, as a function of their center-to-center distance, versus the pertinent parameters of the problem, which are the solvent quality, the grafting-density (number of grafted polymer chains per droplet) and the bulk monomer-concentration. Such an exact study allowed the classification and the determination of the shapes of the effective potentials versus these parameters.

It should be pointed out that considerable scientific investigations have been addressed to Pickering emulsions in the past. In this paper, however, the goal is a review on recent advances dealt with the physical properties of PEs, such as the effective interactions between the clothed oil-droplets, their structure and thermodynamics, cage effect and subdiffusion phenomenon, and spherical diffusion of the anchored nanoparticles onto O/W interface.

This paper is organized as follows. In Sec. 2, we report on the essential static study of the structure and thermodynamics of PEs, which are stabilized by adsorbed charged nanoparticles. A succinct overview of the investigation of the cage effect and subdiffusion within PEs is the aim of Sec. 3. A recall of an exact study of the spherical diffusion of anchored charged nanoparticles is presented in Sec. 4. Finally, some concluding remarks are drawn in the last section.

Static study of structure and thermodynamics

Pair-potential: Consider a suspension of N droplets of a certain liquid that are dispersed in another chemically different liquid (O/W, for instance). The volume of the solution is denoted as V, and their number density as $\rho=N/V$. For simplicity, the droplets are assumed to be *monodisperse* spheres of common diameter σ. The surface of each droplet is wetted by Z irreversibly adsorbed charged nanoparticles of small diameter in comparison with σ. The strong adsorption of the nanoparticles rigidifies the surface of droplets, so that they can be considered as soft spherical charged colloids (as latex balls in water, for instance) that carry the same charge, Ze (macroions), where e is the electron charge. When they are added to the solution, the adsorbed nanoparticles are ionized and release small ions (*counterions*) in the solution. Generally, the colloids are in contact with other *free ions* resulting from a dissociation of an electrolyte (salt, for instance). It is well-known that the surrounding mobile ions lead to a screening of the Coulomb force between charged colloids.

Beside the screened Coulomb interactions, the macroions experience attractive van der Waals forces, and the thermodynamic properties (phase transitions, structure...) of the system can be described correctly within the framework of DLVO theory [52]. In the same context, in his seminal paper [50], I. Sogami used a self-consistent theory (*adiabatic approximation* [65]), combined with a resolution of the Poisson-Boltzmarm equation, which is satisfied by the electric potential created by macroions (ionized latex polyballs), for the determination of their associated effective interaction potential. Such a potential involves a short-range (screened) Coulomb repulsion, whose origin is self-evident, in addition to a long-ranged exponential attractive tail. The Sogami potential has been used to describe the vapor-liquid transition and crystallization of charged colloids observed in experiments [66]. We note that, incidentally, the attractive part of the interaction potential, defined in Eq. (1) (see below), is similar to the (entropic) depletion potential that appears when small-ions (or macromolecules) are interposed between adjacent macroions (or colloids) [67], and the Debye-Hückel screening length then plays the role of the small-ion size (or gyration radius).

The expression of the Sogami-Ise potential between charged oil-droplets reads [50,51]

$$U(r)=\begin{cases}\infty\,, & r<\sigma\,,\\ \dfrac{Z^2e^2}{2\pi\varepsilon_0\varepsilon_r}\left[\dfrac{\sinh(\kappa\sigma/2)}{\kappa\sigma}\right]^2\left(\dfrac{2+\kappa\sigma\coth(\kappa\sigma/2)}{r}-\kappa\right)e^{-\kappa r}\,, & r>\sigma\,.\end{cases} \quad (1)$$

Here, r denotes the center-to-center distance between two interacting charged oil-droplets. In expression above, ε_o is the free space permittivity and ε_r is the relative permittivity of the host liquid (ε_r=80, for water), and the screening parameter κ is defined by

$$\kappa^2=4\pi l_B\sum_i\rho_i z_i^2 \quad (2)$$

where $l_B=e^2/4\pi\varepsilon_0\varepsilon_r k_BT$ stands for the Bjerrum length (l_B=0.7 *nm*, for water, at room temperature), ρ_i for the number density of ions of type i, of common valence z_i, T for the absolute temperature, and k_B for the Boltzmann's constant. The temperature T will be fixed to the value 298 K (room temperature). The Debye-Hückel screening length is $l_D=\kappa^{-1}$. Notice that the Debye approximation remains valid, as long as the condition $\kappa\sigma<1$ is fulfilled. For example, in the presence of a salt of concentration, c_s, the above formula becomes.

$$\kappa^2=4\pi l_B\left(\rho Z^2+c_s\right) \quad (2)$$

Then, the chosen potential depends on *seven* parameters: $(Z,\sigma,\kappa,\varepsilon=\varepsilon_0\varepsilon_r,\rho,c_S,T)$.

It is straightforward to see that the adopted pair-potential vanishes at some known characteristic distance, and exhibits only *one* known minimum that is located in the attraction region, and goes to *zero*, for infinite distances.

Figure 2 shows the variation of the dimensionless pair-potential, $U(t)/k_BT$, upon the dimensionless distance, r/σ, for three values of the dimensionless screening parameter $k=\kappa\sigma$ (by varying the salt-concentration c_s). These curves are drawn with the parameters: $\rho_*=0.005$, $Z=300$ *and* $\sigma=500$ Å. Here, $\rho^*=\rho\sigma^3$ denotes the dimensionless number density.

Finally, we recall that, using this potential, Tata and *coworkers* [68] performed *Monte Carlo* and *Brownian Dynamics* simulations, and the obtained results agree well with certain experimental observations [69,70]. Also Kepler and Fraden [71] determined the pair-potential of the colloidal particles

Citation: Benhamou M, El-Moudny S (2017) Review on Pickering emulsions stabilized by adsorbed nanoparticles: Structure, Thermodynamics, Cage Effect and Subdiffusion. Int J Nanomater Nanotechnol Nanomed 3(2): 057-076. DOI: http://doi.org/10.17352/2455-3492.000022

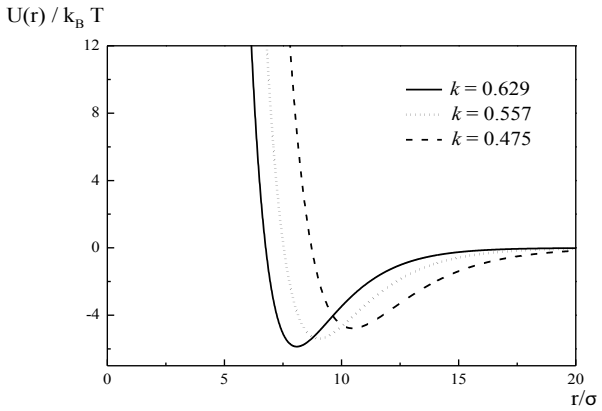

Figure 2: Reduced Sogami-Ise pair-potential, $U(r)/k_BT$, upon the dimensionless distance, r/σ ,for three values of the dimensionless screening parameter, $k=k\sigma$, with the fixed parameters: $p^*= 0.005$, $Z= 300$ and $\sigma =500$ Å.

from measurements of the pair-correlation-function of both dilute and moderately concentrated dispersions. Thus, the determined pair-potential can be reproduced by the Sogami-Ise potential, assuming $c_s = 1.75 \times ?10?^2 1m^{(-3)}$, as pointed out by Tata and Arora [72]. The authors argued that the results by Kepler and Fraden supported the counterion-mediated attraction discussed by Sogami.

Basic equations: Consider a given PE which presents as a suspension of oil-droplets (dispersed phase) in water (continuous phase). These oil-droplets are clothed each by charged nanoparticles that ensure their stabilization, and then prevent the coalescence phenomenon. As we said before, these clothed droplets can be regarded as soft-colloids moving freely in water. Therefore, this PE is considered as a colloidal solution, where the oil-droplets are soft-beads and water is solvent. The investigation of its structural and thermodynamical properties crucially depends on the nature of the mutual interactions between oil-droplets. To this end, use is made of the so-called *Integral Equation Method* (IEM), usually encountered is *Physics of Simple Liquids* [49]. Such a powerful theoretical tool allows the determination of the structure of PEs in a thermodynamic state, characterized by the oil-droplet-density, ρ, bath temperature, T, and a pair-potential, $U(r)$, which expresses the mutual interactions between charged droplets. We note that IEM is a microscopic theory, based on the principles of *Equilibrium Statistical Mechanics* [73].

The basic physical quantity to consider is the structure-factor, $S(q)$, which can be measured using X-rays, neutrons or light scattering experiments. Here, $q = (4\pi / \lambda) sin(\theta / 2)$ denotes the amplitude of the scattering wave-vector, q, which depends on the incident wavelength, λ, and the scattering-angle,θ. The structure-factor, $S(q)$, is nothing else but the Fourier transform of the radial-distribution-function, $g(r)$, where $r \in R^3$ is a three-dimensional vector relating two correlated oil-droplets (one droplet is taken as origin). In fact, the function $g(r)$ traduces the spatial arrangement of the oil-droplets within PE under investigation. Then, we write

$$S(\boldsymbol{q}) = 1 + \rho \int \left[1 - g(\boldsymbol{r})\right] e^{i\boldsymbol{q}.\boldsymbol{r}} d\boldsymbol{r} \tag{3}$$

where ρ accounts for the number density of the oil-droplets. Integral in relation above is performed on the hole real-space, $\boldsymbol{R}^3$. We note that the dependence of the structure-factor, $S(q)$, on the pair-potential is entirely contained in the radial-distribution-function, $g(\boldsymbol{r})$. Therefore, the structural and thermodynamical quantities of PEs depend on the expressions of $g(\boldsymbol{r})$ and $U(r)$. Since, PEs are considered as spatially isotropic liquids, the corresponding structure-factor depends only on the wave-vector modulus, q, and both radial-distribution-function and pair-potential, on distance r.

We write the first important relationship giving the internal energy per oil-droplet, in terms of the radial-distribution-function and pair-potential,

$$E = \frac{3}{2} N k_B T + 2\pi N \int U(r) g(r) r^2 dr \tag{4}$$

The first part of the r.h.s. of the above equality stands for the contribution of an ideal PE (free from interactions).

The second important relationship expresses the dependence of the virial pressure on the PE structure,

$$P = \rho k_B T - \frac{2\pi}{3} \rho^2 \int \frac{dU}{dr} g(r) r^3 dr \tag{5}$$

This is the thermodynamical equation of state of PE.

The last interesting relationship is that relating the structure-factor, at vanishing scattering-angle, and the thermal compressibility, χ_T ,

$$\rho k_B T \chi_T = S(0) = 1 + 4\pi\rho \int \left[1 - g(r)\right] e^{i\boldsymbol{q}.\boldsymbol{r}} r^2 dr \tag{6}$$

Thermodynamically speaking, χ_T^{-1} is directly proportional to the variation of pressure upon the oil-droplet density, i.e.,

$$\chi_T^{-1} = \rho \left(\frac{\partial P}{\partial \rho} \right)_T \tag{7}$$

Then, equality (6) establishes a link between strucrure and thermodynamics.

Of course, all the above relationships necessitate the knowledge of the radial-distribution-function, $g(\boldsymbol{r})$, that crucially depends on the pair-potential between interacting charged oil-droplets, $U(r)$, or equivalently, the total correlation-function, $h(\boldsymbol{r}) = g(\boldsymbol{r}) - 1$. The latter solves the Orstein-Zernike Integral Equation [49]

$$h(\boldsymbol{r}) = c(\boldsymbol{r}) + \rho \int c\left(\left|\boldsymbol{r} - \boldsymbol{r}'\right|\right) h(\boldsymbol{r}') d\boldsymbol{r}' \tag{8}$$

Here, $c(\boldsymbol{r})$ means the direct-correlation-function. Since we are concerned with homogeneous and isotropic PEs, the corresponding functions g, h and c, and the pair-potential U, depend only on the oil-droplet-distance, r, where one droplet is taken as origin. Then, $r \in \boldsymbol{R}^3$ is the position-vector of the second oil-droplet.

The above integral equation, however, contains *two* unknown quantities, which are $h(r)$ and $c(r)$. To solve it, a closure relation between these two quantities is needed. It is convenient to choose IEM with the so-called *Hybridized Mean Spherical Approximation* (HMSA) [74,75]. Its advantage is that, it ensures the *thermodynamic consistency* in calculating the internal compressibility by two different ways, definitions

Citation: Benhamou M, El-Moudny S (2017) Review on Pickering emulsions stabilized by adsorbed nanoparticles: Structure, Thermodynamics, Cage Effect and Subdiffusion. Int J Nanomater Nanotechnol Nanomed 3(2): 057-076. DOI: http://doi.org/10.17352/2455-3492.000022

(6) and (7). For simple fluids, such a mixing IEM was solved using some numerical algorithm combined with the iterations techniques [76,77].

Structural properties: To investigate quantitatively these properties, use is made of IEM with HMSA, which allows the determination of the radial-distribution-function, $g(r)$, the structure-factor, $S(q)$, the pressure, P, the (internal) energy, E, and the thermal compressibility, xt. Naturally, the three last thermodynamical properties will be compared to their counterparts relatively to an ideal PE (without interactions), namely $P_0 = k_B T \rho$, $E_0 = 3Nk_B T / 2$, and $\chi_T^0 = P_0^{-1} = (k_B T \rho)^{-1}$.

All computations are achieved adopting Sogami-Ise potential, relation (1). In this study, the salt-concentration is fixed to $c_s = 1.75 \times 10^{21}\, m^{-3}$, and the absolute temperature, T, to its room value. But the remaining parameters (surface valence of oil-droplets), σ (oil-droplet-size) and ρ (oil-droplet-density) will be varied systematically. Discussion will be done considering the dimensionless variables: r/σ, $q\sigma$, $\rho^* = \rho\sigma^3$.

More details about this study can be found in Ref. [48]

A. Density effects

Here, the diameter of the oil-droplets, σ, and their surface charge, Ze, are fixed to the values: $\sigma = 20000$ Å and $Z = 20000$. These two parameters are mainly controlled by the concentration of the anchored charged nanoparticles on the surface of the oil-droplets. The density of the oil-droplets, ρ, will be varied. We note that the chosen values of density are those used in some recent experiment study [78].

Figure 3a shows the variation of the correlation-function, $g(r)$, against the dimensionless distance, r/σ, for various values of the dimensionless density, ρ^*. First, remark that, as expected, the (principal) peak-height of the correlation-function becomes more and more pronounced with increasing dimensionless number density, ρ^*. Such a result indicates that, when the number density of the clothed oil-droplets is increased, the local density around an oil-droplet, taken as origin, also increases. This means that the dispersion is more ordered by an increase of the droplet-density. Second, the position of the principal peak is shifted toward its smaller values, when the droplet density is increased. This can be explained by the fact that an increase of this density leads to a reduction of the inter-distance between oil-droplets (strong correlations). This tendency has been observed in several previous studies [79-82].

Figure 3b shows the structure-factor, $S(q)$, versus the dimensionless scattering wave-vector amplitude, $q\sigma$, for the same values of the dimensionless number density as in figure 3a. The conclusions are the same, as before, except for the position of the principal peak that is rather shifted to its higher values, as the oil-droplet density is increased. This fact is not surprising, since the wave-vector amplitude, q, is dimensionally the inverse of a distance.

B. Charge effects

Now, the aim is to quantify the influence of the charge carried by the dispersed oil-droplets on the structure of the considered PE. Their size and dimensionless density were fixed to the values: σ = 20000 Å and ρ_*= 0.0020.

Figure 4a shows the dimensionless Sogami-Ise pair-potential, $U(r)/k_B T$, versus the dimensionless distance, r/σ, for three values of the charge parameter Z, fixing the other parameters to the values: ρ_*= 0.0020, σ = 20000 Å and κ = 0.25. These curves clearly indicate that the potential-depth is diminished by an increasing of the surface charge. In other words, the potential becomes less attractive, by an augmentation of the charge that ensures more stable emulsions, due to the electrostatic repulsion. Such a tendency is confirmed in figures 4b,c representing the correlation-function and the structure-factor, respectively. Remark that the position of the principal peak of the correlation-function is shifted toward its higher values, as the surface charge is increased. In contrary, that of the structure-factor becomes less important. This can be understood by the fact that the size of the local ordered region made of first neighbors (principal peak position), is more and more larger, as the surface charge is augmented, due to the repulsion of the charged droplets. In addition, Figure 4b indicates that the height of the principal peak of the correlation-function increases, as the charge increases. Finally, we emphasize that the correlation-function and the structure-factor shapes are in agreement with MC simulations [83].

C. Size effects

To quantify the effects of the droplet-size on the structure of PEs, the surface charge of the droplets and their dimensionless density are fixed to the values: Z= 2000 and ρ^*= 0.0020, and their size will be varied.

Figure 5a shows the shapes of the pair-potential versus distance, for several values of the droplet-size. According to these curves, the potential-depth diminishes, and the position of its minimum is shifted toward its higher values, by a progressive increase of this size. This indicates that the emulsion becomes more and more repulsive for larger droplets.

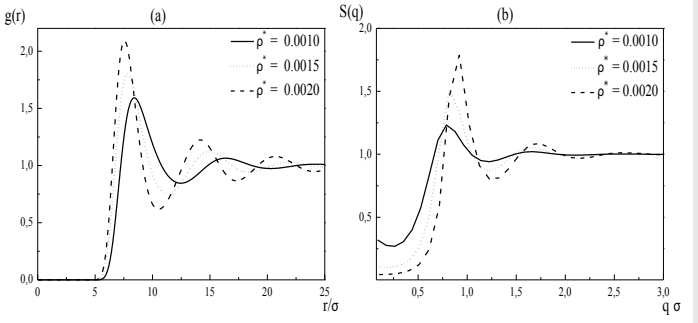

Figure 3: (a) Correlation-function, g(r), upon the dimensionless distance, r /σ, and (b) structure-factor, S(q), versus the dimensionless scattering wave-vector amplitude, qσ, for various values of the dimensionless number density, ρ*.

Citation: Benhamou M, El-Moudny S (2017) Review on Pickering emulsions stabilized by adsorbed nanoparticles: Structure, Thermodynamics, Cage Effect and Subdiffusion. Int J Nanomater Nanotechnol Nanomed 3(2): 057-076. DOI: http://doi.org/10.17352/2455-3492.000022

On the other hand, Figure 5b clearly shows that the height of the principal peak of the correlation-function decreases progressively, and its position is shifted toward its higher values with increasing droplet-size. Then, the size of the local ordered region made of first neighbors (around some given droplet) increases with increasing droplet-diameter. Such a figure also shows that the mean-distance between the dispersed droplets is diminished by an augmentation of their size. This tendency is confirmed by Figure 5c that represents the evolution of the structure-factor, for different values of the droplet-size. We emphasize that such a behavior agrees with those results from MC simulations [83].

Thermodynamical properties: We have seen above that the structure of PEs is substantially influenced by a change of the pertinent factors (density, surface charge, size). It is the same for their thermodynamical properties, as pressure, internal energy, and thermal compressibility, since structure and thermodynamics are intimately related, equalities (4) to (6). The aim of this paragraph is to recall how these thermodynamical properties can be modified under a change of these parameters. Here, the bath temperature is fixed.

A. Charge effects: We start with the evolution of the pressure, knowing the simulated correlation-function and the expression of the pair-potential between the interacting oil-droplets. The variation of the (reduced) pressure, upon droplet-density, is depicted in figure 6a, for various values of the surface charge. Remark that the pressure curve presents two density-regimes. The first corresponds to low-densities less than an unique minimum, which is sensitive to the variation of the surface charge. For high-densities, however, the pressure increases (as expected).

Now, the question is addressed to the internal energy, usually chosen as the thermodynamical potential for the colloidal suspensions studied by IEM, instead of the free energy. But the later can be obtained integrating the pressure with respect to volume (or equivalently with respect to density). Hence, the increasing of stability of the system must be discussed in term of the internal energy. Denote by $\Delta E = E - E_0$, the shift of the real internal energy, E, from that of an ideal emulsion, $E_0 = 3Nk_BT/2$, or simply *excess internal energy*. Figure 6b shows the evolution of the (reduced) internal energy with the droplet-density, for several values of the

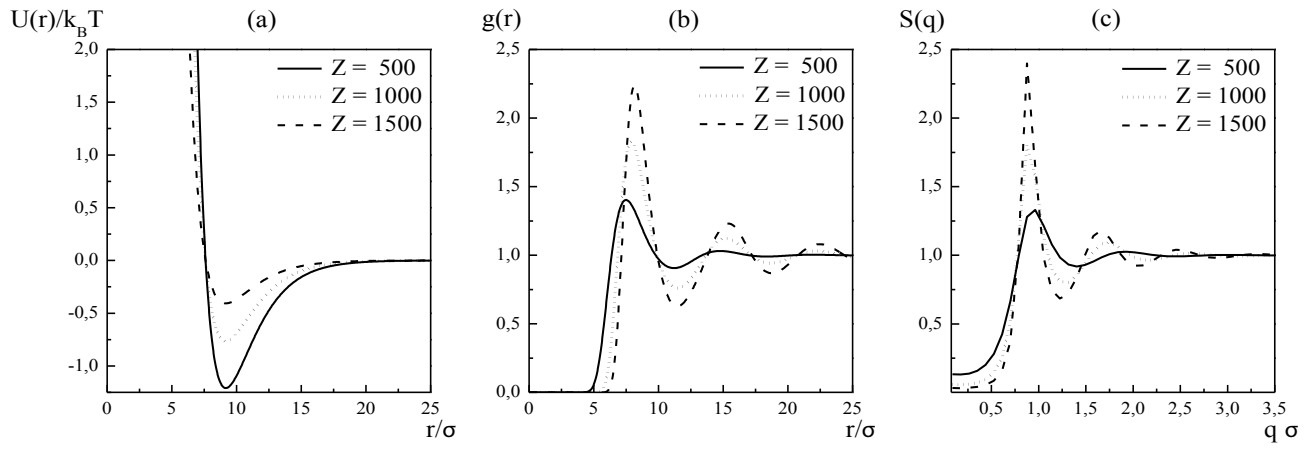

Figure 4: (a) Reduced Sogami-Ise pair-potential, $U(r)/k_BT$, upon the dimensionless distance, r / σ, (b) correlation-function, g(r), upon the dimensionless distance, r / σ, and (c) structure-factor, S (q), versus the dimensionless scattering wave-vector amplitude, qσ, for some values of the droplet surface charge, Z, keeping fixed the other parameters.

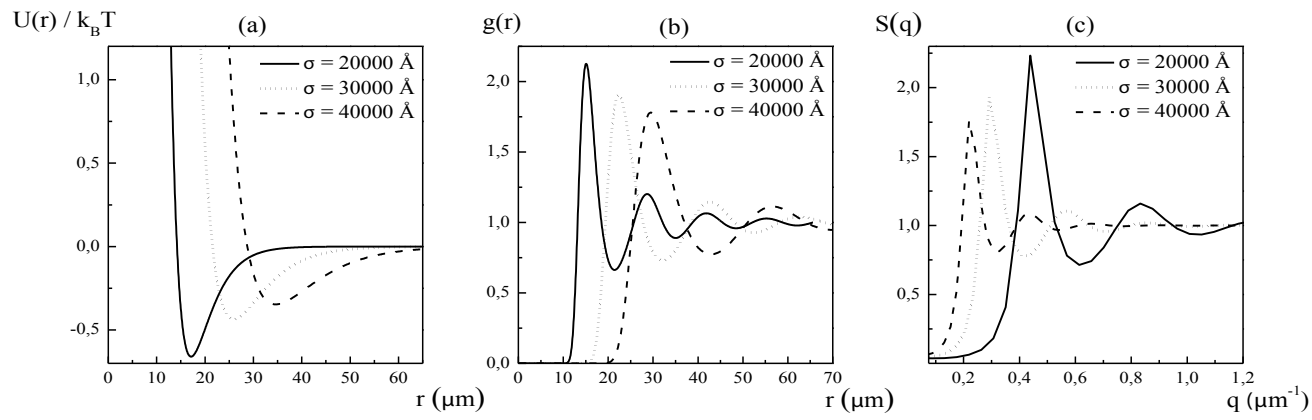

Figure 5: (a) Reduced Sogami-Ise pair-potential, $U(r)/k_BT$, upon distance, r, (b) correlation-function, g(r), upon distance, r, and (c) structure-factor, S (q), versus the scattering wave-vector, q, for various values of the droplet-size, σ, keeping fixed the other parameters.

Citation: Benhamou M, El-Moudny S (2017) Review on Pickering emulsions stabilized by adsorbed nanoparticles: Structure, Thermodynamics, Cage Effect and Subdiffusion. Int J Nanomater Nanotechnol Nanomed 3(2): 057-076. DOI: http://doi.org/10.17352/2455-3492.000022

surface charge. These curves indicate that the energy exhibits a minimum that strongly depends on the droplet surface charge. Then, PEs are more stable by the presence of strong charges.

The last quantity to consider is the thermal compressibility, as a function of the droplet-density, keeping fixed the remaining parameters. Its variation is shown in figure 6c, for different values of the surface charge of the droplets. This figure tells us that the thermal compressibility admits *one* maximum (for low-densities), of which the location and intensity are very sensitive to the variation of the charge carried by the droplets. Remark that the position of this maximum is shifted toward its higher values, and the maximal intensity is diminished, as the surface charge is increased. But for high-densities, the variation of the charge does not affect the (almost linear) decay of the thermal compressibility with density.

Typical magnitudes of pressure, internal energy and thermal compressibility are given in Ref. [48], versus some values of the surface charge.

B. Size effects: The first thermodynamical quantity to consider is the pressure, and we are interested in its variation upon the droplet-density. Such a variation is reported in figure 7a, for several values of the droplet-size. Remark that, as before, the pressure curve exhibits two regimes. The first corresponds to the lower values of density less than an unique minimum of the pressure, which is weakly sensitive to the variation of the droplet-size, and much more prominent for the smallest-size droplets. In the second regime, however, the pressure monotonously increases with density (as expected).

The second question is addressed to the evolution of the internal energy versus the density of the droplets, for different values of their size. This evolution is drawn in figure 7b, and remark that the internal energy admits an unique minimum, which strongly depends on the droplet-size. Then, the emulsion is rather more stable for smaller droplets.

The last thermodynamical quantity to consider is the thermal compressibility, and we are concerned with its variation upon the density of the droplets, for several values of their size. Figure 7c shows this variation indicating that the thermal compressibility passes by a maximum, which is strongly sensitive to the variation of the droplet-size, from

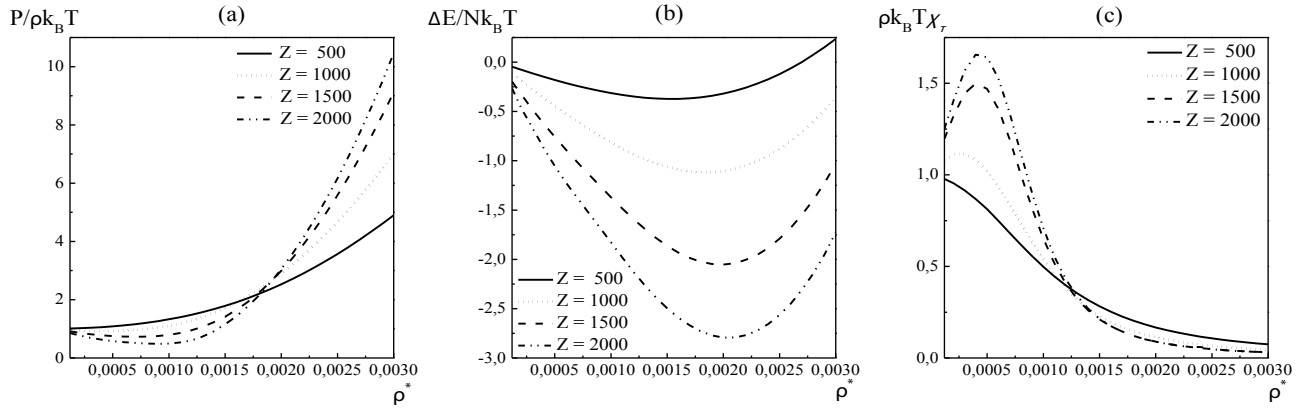

Figure 6: (a) Reduced pressure, P/ k_BTρ, (b) reduced excess internal energy, ΔE / Nk_BT, and (c) reduced thermal compressibility, ρk_BTxT, versus the density of the droplets, for various values of their surface charge.

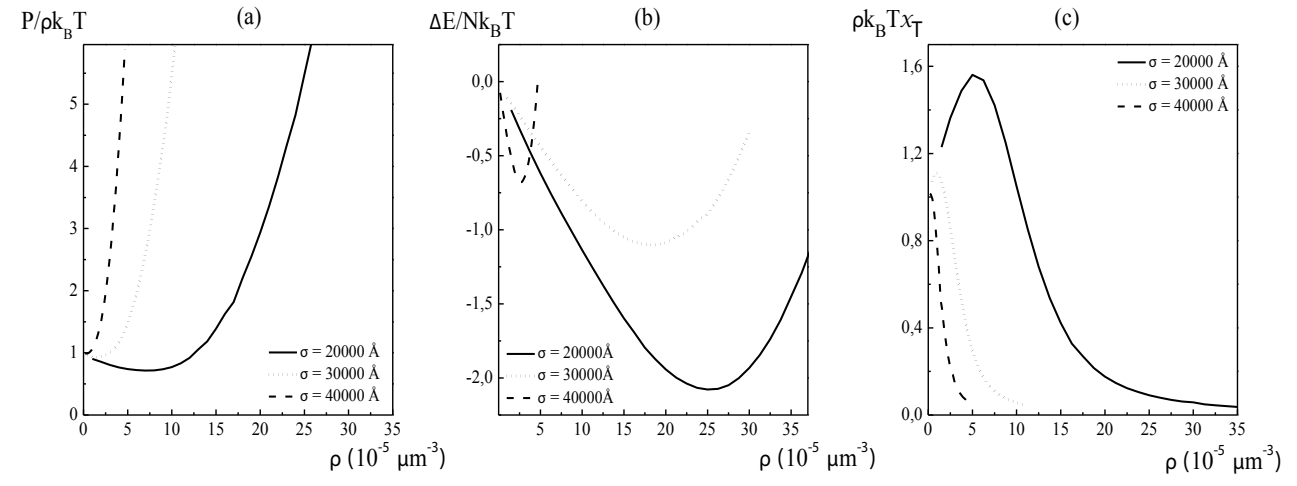

Figure 7: (a) Reduced pressure, P/ k_BTρ, (b) reduced excess internal energy, ΔE / Nk_BT, and (c) reduced thermal compressibility, ρk_BTxT, versus the density of the droplets, for various values of their size.

Citation: Benhamou M, El-Moudny S (2017) Review on Pickering emulsions stabilized by adsorbed nanoparticles: Structure, Thermodynamics, Cage Effect and Subdiffusion. Int J Nanomater Nanotechnol Nanomed 3(2): 057-076. DOI: http://doi.org/10.17352/2455-3492.000022

position and intensity point of view. For high-densities, however, a variation of the size does not affect the decay of the thermal compressibility, as the droplet-density is increased.

Typical magnitudes of pressure, internal energy and thermal compressibility are given in Ref. [48], choosing some values of the droplet-size.

Study of cage effect and subdiffusion

Introduction: In this introductory section, we present a bibliographic note on the subdiffusion phenomenon appearing in complex systems, as PEs, and precise the main goal. We recall that the subdiffusion movement of the dispersed oil-droplets within PEs was extensively studied in Ref. [54].

Due to the thermal agitation, the clothed oil-droplets execute a lateral diffusion with the molecules of water. At the beginning, a single droplet normally diffuses, but at large-time, this motion is hampered by the presence of the other neighboring oil-droplets. As consequence, a given oil-droplet executes rather an anomalous diffusion we are interested in. As shown below, this anomalous phenomenon crucially depends on the pertinent factors, which are the (surface) charge carried by the droplets, their size and density, and the salt-concentration.

The anomalous diffusion in various fields of science (physics, chemistry, biology, ecology...) has received much attention from a theoretical and experimental point of view. In fact, such a diffusion appears in heterogeneous, disordered, fractal, colloidal and polymer systems, and in general, it produces within the complex systems containing entities that move on different scale-times. In opposition to the normal or Brownian diffusion, the anomalous diffusion is more slower, due to an extreme difficulty that a particle (*tracer*) moves in a complex structure. This kind of diffusion is usually referred to as *subdiffusion*, and it is characterized by a mean-square-displacement that behaves as

$$W(t) = \langle (r(t) - r(0))^2 \rangle = 2D_\alpha t^\alpha \ . \ (0 < \alpha < 1) \qquad (9)$$

This large-time behavior then deviates from the linear dependence on time found for the Brownian motion [84-86]. In expression above, ***r(t)*** represents the time-position of the random walker, and the generalized diffusion coefficient, D_a, also called "fractional diffusion coefficient", is expressed in $length^2 / time^\alpha$ unit.

We emphasize that the sub diffusion is a feature of the *crowded* system, where the trajectories of their mobile constituents are strongly correlated. Notice that the above scaling relation is valid for large-times that is beyond some characteristic time depending on the specific details of the diffusion process and the structure of the host medium. In general, a particle is said to be subdiffusive if the condition $W(t)/t \to 0$, for $t \to +\infty$, is satisfied (very slow diffusion). This explains why the exponent α must be in the interval $0 < \alpha < 1$.

It is noted that the subdiffusive transport appears in a variety of systems, such as the random-walk in fractal structures [85], fractional-time Brownian motion [87], living systems [88], charge carrier transport in amorphous semiconductors [89,90], NMR diffusometry on percolation structures [91], and the motion of a colloid in a polymer network [92]. For example, for diffusion in fractal structures, $\alpha = 2/d_w$, where $d_w > 2$ is the *walk-dimension* ($d_w = 2d_f / d_s$, where d_f and d_s are the fractal and spectral dimensions, respectively), and for the fractional-time Brownian motion, $\alpha = 2H$, where H is the *Hurst index*. Examples of enhanced diffusion $(\alpha > 1)$ include tracer particles in vortex arrays in a rotating flow [93], layered velocity fields [94], and Richardson diffusion [95]. The case $1 < \alpha < 2$ refers to *superdiffusion* (turbulent plasmas, Levy-flights, transport in polymers), $\alpha = 2$, to *ballistic diffusion* (optical traps), and $\alpha = 3$, to *Richardson diffusion* (atmospheric turbulence). The subdiffusion or superdiffusion exponent, α, is not a universal quantity, but mainly depends on the pertinent parameters that control the phenomenon. As we shall see below, for the subdiffusion of the clothed droplets, this exponent shall depend on their size, density and surface charge, and the salt-concentration.

In a very recent work [53], a quantitative study of the subdiffusion phenomenon within PEs was achieved, using *Molecular Dynamics* (MD) simulations. We recall that this kind of computational method was introduced by Alder and Wainwright [96], for the investigation of the structure and dynamics of liquids. Within the framework of MD simulations, the dynamic properties are investigated through the time-evolution of the mean-square-displacement (MSD), combined with the velocity auto-correlation function (VACF). In particular, the latter informs on the appearance of the cage effect within complex media.

For the study of the cage effect and subdiffusion within PEs, the authors of Ref. [53] have adopted the Sogami-Ise [50,51] pair-potential between the charged clothed oil-droplets (Eq. (1)), and applied MD techniques, for the computation of both MSD and VACF, from which the transport coefficients were extracted.

From an experimental point of view, the subdiffusion was observed in many different areas of science. Crowded biological media [97-102], electrons in porous media [103], colloidal suspensions under certain conditions [104-108] and granular materials [109] constitute particular examples.

For the dynamics study (subdiffusion) in relation with PEs, the starting point was a proposition of a dynamic theory [53], based on a generalized Langevin equation (with memory). This integro-differential equation is solved by VACF, which is intimately related to MSD (see below). The exact solution of this equation, with an appropriate choice of the memory-function, enables one the validation of the results form MD, as a computer experiment.

Dynamic theory

Normal diffusion: Consider a given oil-droplet with anchored charged nanoparticles, termed *tracer* or *random walker*, which executes a diffusion movement in the continuous phase (water). For early times, this diffusion is normal, due to

Citation: Benhamou M, El-Moudny S (2017) Review on Pickering emulsions stabilized by adsorbed nanoparticles: Structure, Thermodynamics, Cage Effect and Subdiffusion. Int J Nanomater Nanotechnol Nanomed 3(2): 057-076. DOI: http://doi.org/10.17352/2455-3492.000022

the absence of the correlations. This means that the random walker is not yet trapped in a cage. The existence of such a regime was demonstrated by computer simulations in Ref. [53], for small-times.

We recall that the Brownian motion of a random walker (a droplet, in our case) is well-described by the classical Langevin equation

$$M\frac{d\boldsymbol{v}(t)}{dt} = -\zeta \boldsymbol{v}(t) + \boldsymbol{F}_s(t) \tag{10}$$

Here, M denotes the mass of the random walker, $\boldsymbol{v}(t) \in \boldsymbol{R}^3$ is its velocity, ζ is the *friction coefficient*, and $F_s(t)$ represents a *stochastic force*. We recall that the friction coefficient, ζ, is related to the viscosity of the emulsion, η, and the oil-droplet radius, R, by the classical Stokes' relation, $\zeta = 6\pi\eta R$. Naturally, the viscosity of the solution depends on the number density of the dispersed oil-droplets, ρ. For small values of the density, this effective viscosity obeys the well-known law [110],

$$\eta(\rho) = \eta_W\left(1 + 5\frac{\eta_O - \eta_W}{2\eta_O + 3\eta_W}\rho^*\right), \quad (\rho^* \ll 1) \tag{11}$$

where $\rho^* = \rho\sigma^3$ denotes the reduced oil-droplet number density (or oil-droplet volume fraction), $_w$ is the viscosity of water, and η_o is that of oil. As it should be, we have the inequality $\eta(\rho) > \eta_W$, since $\eta_O > \eta_W$.

There, the stochastic force is considered to be a white noise, with

$$\langle \boldsymbol{F}_S(t)\rangle = 0 \tag{12a}$$

$$\langle \boldsymbol{F}_S(t).\boldsymbol{F}_S(0)\rangle = 6k_B T\zeta\delta(t) \tag{12b}$$

with the Dirac distribution, $\delta(t)$. The brackets $\langle ...\rangle$ mean an average over time. For two dynamic variables A and B, their individual average and time correlation-function are defined as follows

$$\langle A(t_0)\rangle = \lim_{\tau\to\infty}\frac{1}{\tau}\int_0^\tau dt A(t+t_0) \tag{13a}$$

$$\langle A(t_1)B(t_0)\rangle = \lim_{\tau\to\infty}\frac{1}{\tau}\int_0^\tau dt A(t+t_1)B(t+t_0) \tag{13b}$$

Here, τ is the time-interval, in which the quantities A and B are measured. We note that for dynamic systems that are very close to the thermodynamic equilibrium (*stationary stochastic processes*), the mean-value $\langle A(t_0)\rangle$ does not depend on its argument, $t_{0,}$ and then, the correlation-function $\langle A(t_1)B(t_0)\rangle$ depends only the time difference $t_1 - t_0$.

In addition to equalities (12a) and (12b), we have

$$\langle \boldsymbol{v}(0).\boldsymbol{F}_S(t)\rangle = 0 \tag{14}$$

This is the so-called *orthogonality relation* traducing the fact that $\boldsymbol{F}_s(t)$ is a stochastic force, and it must not be correlated with the velocity of the tracer, at another time.

The basic dynamic quantities of our interest are VACF, $\langle \boldsymbol{v}(t).\boldsymbol{v}(0) = c_{vv}(t)$, and MSD, $\langle (\boldsymbol{r}(t) - \boldsymbol{r}(0))^2\rangle \equiv W(t)$. Notice that these quantities are not independent each other (see below).

VACF solves the following simple differential equation [111].

$$\frac{dc_{vv}(t)}{dt} = -\gamma c_{vv}(t) \tag{15}$$

whose solution is

$$c_{vv}(t) = \langle \boldsymbol{v}^2\rangle e^{-\gamma t}, \quad \langle v^2\rangle = c_{vv}(0) = 3k_B T / M \tag{16}$$

with the mass weighted friction constant $\gamma = \zeta / M$, called *relaxation rate*.

On the other hand, VACF and MSD are generally related by [111]

$$W(t) = \int_{t_0}^{t} dt_1 \int_{t_0}^{t_1} dt_2 c_{vv}(t_1, t_2) = 2\int_{t_0}^{t} dt'(t - t')c_{vv}(t') \tag{17}$$

Also, it straightforward to show that MSD and VACF are related by [111]

$$c_{vv}(t) = \frac{1}{2}\frac{d^2W(t)}{dt^2}. \quad (t > 0) \tag{18}$$

Now, combining expression (16) of VACF with basic relations (17) or (18) gives the time-evolution of MSD [111],

$$W(t) = 6\frac{k_B T}{M}\left(\frac{e^{-\gamma t} - 1 + \Upsilon t}{\gamma^2}\right) \tag{19}$$

For times much greater than the inverse *relaxation rate* $(t \gg \gamma^{-1} \equiv t^*)$, MSD grows linearly, and we have

$$W(t) = 6Dt, \quad (t \gg t^*) \tag{20}$$

with the diffusion coefficient

$$D = \frac{k_B T}{M\gamma} = \frac{k_B T}{\zeta} \tag{21}$$

This is the standard *Einstein relation* that expresses a compromise between the thermal fluctuations (through the thermal energy $k_B T$) and the dissipation (via the friction coefficient ζ). Then, the linear growth of MSD, versus time, is reached beyond the characteristic time

$$t^* = \gamma^{-1} = \frac{M}{6\pi\eta(\rho)} \tag{22}$$

The characteristic time, t^*, depends only on the droplet-density, through the viscosity, $\eta(\rho)$, relation (11). For small-times, that is for $t \ll t^*$, the factor $e^{-\gamma t}$ can be approximated by $1 - \gamma t + \gamma^2 t^2 / 2$, and one finds

$$W(t) = \langle \boldsymbol{v}^2\rangle t^2 = 3(k_B T / M)t^2, \quad (t \ll t^*) \tag{23}$$

This small-time behavior shows that MSD grows with time as t^2. Then, in the initial phase, MSD is parabolic, and the oil-droplets execute rather a *ballistic motion*.

B. Anomalous diffusion

Generalized Langevin equation: Now, the raised question is how a random walker (a given droplet) diffuse in water, beyond the relaxation rate, t^*. In this time-regime, the random walker (*target*) feels to be trapped in a cage formed by other oil-droplets (*traps*), and then, it cannot escape from this cage, only after a long-time. We denote by N_c, the average-number of traps around the considered random walker. Consequently, the presence of the traps makes difficult such a diffusion process, and then, the random walker executes rather a subdiffusion,

Citation: Benhamou M, El-Moudny S (2017) Review on Pickering emulsions stabilized by adsorbed nanoparticles: Structure, Thermodynamics, Cage Effect and Subdiffusion. Int J Nanomater Nanotechnol Nanomed 3(2): 057-076. DOI: http://doi.org/10.17352/2455-3492.000022

characterized by an exponent, α. The latter naturally depends on the essential factors governing dynamics, namely, the charge carried by the oil-droplets, and their density, and the concentration of salt in solution. Here, the bath temperature, *T*, is fixed to its room value. As demonstrated by MD simulations [53], before the subdiffusion takes place, there exists a time-interval we shall precise below, over which MSD is independent of time (plateau-regime), and VACF exhibits oscillations.

To investigate quantitatively the cage effect and the subdiffusion phenomenon, the authors of Ref. [53] started from a generalized Langevin equation (GLE) [111], developed in the past by Zwanzig [112]. GLE that is an extension of the standard Langevin equation (10), where the friction is assumed to be determined by the instantaneous velocity of the particle. Then, GLE describing the motion of the random walker, reads

$$\frac{d\boldsymbol{v}(t)}{dt} = -\gamma \boldsymbol{v}(t) - \int_{t_0}^{t} \kappa(t-t')\boldsymbol{v}(t') + \boldsymbol{F}_s(t) \qquad (24)$$

Here, $\boldsymbol{v}$ stands for the velocity of the moving tracer, $\gamma = \zeta / M$ for the relaxation rate (ζ is the friction coefficient and *M* is the mass of the tracer), and κ for the memory-function that expresses the friction retardation, which must not be confused with the Coulomb screening parameter appearing in the pair-potential expression (1), and $\boldsymbol{F}_{ss}(t)$ (with $t > 0$) is a random force felt by the moving oil-droplet due to its collisions with the molecules of the surrounding liquid (water). We note that this random force also satisfies equalities (12a) and (14), but with a non-trivial second moment,

$$\langle \boldsymbol{F}_S(t).\boldsymbol{F}_S(0)\rangle = 6Mk_BT\left[\gamma\delta(t) + \kappa(t)\right], \quad (t > 0) \qquad (25)$$

which is a generalization of Eq. (12b).

We emphasize that the basic relationships (17) and (18) between MSD and VACF remains valid for memory-diffusion-processes, but equality (15) becomes

$$\frac{dc_{vv}(t)}{dt} = -\gamma c_{vv}(t) - \int_{t_0}^{t} dt'\kappa(t-t')c_{vv}(t') \qquad (26)$$

This is an integro-differential equation solved by VACF, knowing the form of the memory-function, $\kappa(t)$.

Oscillating regime: Beyond the normal diffusion regime, the random walker is subject to oscillations before it undergoes a subdiffusion process. Therefore, the tracer moves in a harmonic potential resulting from its interactions with its nearest neighbors. This is equivalent to take, for the memory-function, the following form

$$\kappa(t) = \omega_0^2\theta(t) \qquad (27)$$

Here, $\theta(t)$ denotes the *Heaviside step function*. The frequency ω_0 must be considered as a phenomenological parameter that depends, of course, on the essential factors, which are the surface charge of the oil-droplets, *Ze*, their number density, ρ, and the salt-concentration, c_s. Intuitively, the frequency ω_0 increases with increasing Z and ρ and decreasing c_s. In particular, we expect that this frequency scales with the valence *Z* as $\omega_0 \sim Z$. The form (27) is attributed to the so-called *Langevin oscillator*.

With the particular memory-function (27), the integro-differential (26) becomes

$$\frac{dc_{vv}(t)}{dt} = -\gamma c_{vv}(t) - \omega_0^2 \int_{t_0}^{t} dt' c_{vv}(t') \qquad (28)$$

Then, the dynamic model depends on *two* phenomenological parameters that are the relaxation rate $\gamma > 0$ and frequency $\omega_0 > 0$ of the Langevin oscillator.

To derive the expressions of VACF and MSD upon time, use was made of the Laplace transform (LT) [53]. We recall that, for an arbitrary function, $f(t)$, defined for $t \geq 0$, the corresponding LT writes

$$\hat{f}(s) = \int_0^{\infty} e^{-st} f(t) \qquad (29a)$$

The inverse LT is

$$f(t) = \frac{1}{2\pi i}\oint_c e^{st}\hat{f}(s) \qquad (29b)$$

where *C* is an integration contour in complex-plan *C*, with *Re*[*s*] >0. We recall that LT of a convolution product (*f* * *g*) (*t*) is simply $\hat{f}(s) \times \hat{g}(s)$.

Laplace transforming of basic equation (28) yields

$$c_{vv}(s) = \langle v^2\rangle \frac{s}{s^2 + \Upsilon s + \omega_0^2} = \langle v^2\rangle \frac{s}{(s-s_1)(s-s_2)}, \quad c_{vv}(0) = \langle v^2\rangle, \qquad (30)$$

with the two complex poles

$$s_{1,2} = -\frac{\gamma}{2} \pm i\tilde{\omega} \qquad (30a)$$

where the characteristic frequency, $\tilde{\omega}$, is given by

$$\tilde{\omega} = \sqrt{\omega_0^2 - \frac{\gamma^2}{4}}, \quad (\gamma < 2\omega_0) \qquad (30b)$$

VACF is then obtained by the inverse LT, using the contour integral,

$$c_{vv}(t) = \langle v^2\rangle e^{-\gamma t/2}\left\{\cos(\tilde{\omega}t) - (\gamma/2\tilde{\omega})\sin(\tilde{\omega}t)\right\}, \quad (\gamma < 2\omega_0) \qquad (31)$$

Therefore, for high-frequencies, that for $\omega_0 > \gamma/2$, VACF is a quasi-periodic function of time. This is the *underdamped regime*. For low-frequencies $(\omega_0 < \gamma/2)$, however, VACF does not oscillate and is given by

$$c_{vv}(t) = \langle v^2\rangle e^{-\gamma t/2}\left\{\cosh(\hat{\omega}t) - (\gamma/2\hat{\omega})\sinh(\hat{\omega}t)\right\}, (\gamma > 2\omega_0) \qquad (32)$$

with the notation

$$\hat{\omega} = \sqrt{\frac{\gamma^2}{4} - \omega_0^2}, \quad (\gamma > 2\omega_0) \qquad (32a)$$

This is the *overdamped regime*. For intermediate-frequencies $(\gamma = 2\omega_0)$, marking the passage from the oscillating behavior to the non-periodic one, VACF is simply given by

$$c_{vv}(t) = \langle v^2\rangle e^{-\gamma t/2}(1 - \gamma t/2), \quad (\gamma = 2\omega_0) \qquad (33)$$

This is the *critical regime*.

Also, MSD can be calculated using LT. Combining Eqs. (18) and (30) yields

$$\hat{W}(s) = \langle v^2\rangle \frac{1}{s(s-s_1)(s-s_2)} \qquad (34)$$

Citation: Benhamou M, El-Moudny S (2017) Review on Pickering emulsions stabilized by adsorbed nanoparticles: Structure, Thermodynamics, Cage Effect and Subdiffusion. Int J Nanomater Nanotechnol Nanomed 3(2): 057-076. DOI: http://doi.org/10.17352/2455-3492.000022

An inverse LT gives

$$W(t)=6\frac{k_BT}{M\omega_0^2}\left[1-e^{-\gamma t/2}\left\{cos\left(\tilde{\omega}t\right)+\left(\gamma/2\tilde{\omega}\right)sin\left(\tilde{\omega}t\right)\right\}\right]\ ,\ \left(\gamma<2\omega_0\right) \tag{35}$$

for the overdamped regime,

$$W(t)=6\frac{k_BT}{M\omega_0^2}\left[1-e^{-\gamma t/2}\left\{cosh\left(\hat{\omega}t\right)+\left(\gamma/2\hat{\omega}\right)sinh\left(\hat{\omega}t\right)\right\}\right]\ ,\ \left(\gamma>2\omega_0\right) \tag{36}$$

for the underdamped regime, and

$$W(t)=6\frac{k_BT}{M\omega_0^2}\left\{1-e^{-\gamma t/2}\left(1+\gamma t/2\right)\right\}\ ,\ \left(\gamma=2\omega_0\right) \tag{37}$$

for the critical regime.

As it should be, in the limit $\omega_0\to 0$, results (16) and (19) are recovered.

Contrary to the normal Brownian diffusion, MSD approaches its plateau value, in the $t\to\infty$ limit, independently of the dynamic regime,

$$W(t)=6\frac{k_BT}{M\omega_0^2}\ ,\ \left(t\gg 2\gamma^{-1}\equiv t^{**}\right) \tag{38}$$

Then, this corresponds to a vanishing diffusion exponent, that is $\alpha_p=0$. Notice that the second characteristic time, *t*** , is *two* times the time *t**, defined in Eq. (22), that is $t^{**}=2t^{*}$.

Subdiffusive regime: Beyond the plateau regime, the tracer follows a slow motion, and the large-time behavior of its MSD is defined in relation (9). Notice that the normal diffusion, with $W(t)\sim t$ (large-time), corresponds to a vanishing VACF, that is $c_{vv}(t)=0$ (large-time), whereas $c_{vv}(t)\neq 0$, for an anomalous diffusion. Specifically, $c_{vv}(t)<0$ corresponds to a subdiffusion (since *a* < 1), and $c_{vv}(t)>0$, to a superdiffusion (since *a* > 1). The property $c_{vv}(t)<0$, at large-time, implies that MSD is a *concave* function. Physically speaking, the negativity of VACF, for large-time, indicates a persistence tendency of the diffusive oil-droplet to invert its direction of motion and to stay localized. This is due to the fact that the survival probability is not zero.

Combing general relationship (18) with MSD behavior (9) gives

$$c_{vv}(t)=\alpha(\alpha-1)D_\alpha t^{\alpha-2}\ ,\ \left(t\to\infty\right) \tag{39}$$

Remark that, contrary to the normal diffusion, for which VACF exponentially fails, at infinity that relatively to the subdiffusion is long-ranged. From the above asymptotic behavior, the generalized diffusion coefficient, D_a, is deduced,

$$D_\alpha=\frac{1}{\alpha(\alpha-1)}\lim_{t\to\infty}\left[\frac{c_{vv}(t)}{t^{\alpha-2}}\right] \tag{40}$$

In the same sense, it was demonstrated [113] that the fractional diffusion coefficient D_a is given by a generalized Green-Kubo formula

$$D_\alpha=\frac{1}{\Gamma(\alpha+1)}\int_0^\infty dt\,{}_0\hat{\partial}_t^{\alpha-1}c_{vv}(t)\ ,\ \left(0<\alpha<1\right) \tag{41}$$

where

$${}_0\hat{\partial}_t^{\alpha-1}c_{vv}(t)=\frac{d}{dt}\left[\int_0^t dt'\left(t-t'\right)^{\alpha-1}c_{vv}(t')\right] \tag{42}$$

is the *fractional Riemann-Liouville derivative* [114] of order 1 - *a* of function $c_{vv}(t)$, and $\tilde{A}(x)$ is the *Euler gamma function*. For normal diffusion (a = 1), the usual Green-Kubo formula is then recovered,

$$D_\alpha=\int_0^\infty dt c_{vv}(t)\ ,\ \left(\alpha=1\right) \tag{42a}$$

Laplace transforming integro-differential equation (28) and using a Tauberian theorem due to Hardy, Littlewood and Karamata [113], which establish a relation between slowly growing functions an their LT, leads to the large-time behavior of the (positive) memory-function [113]

$$\kappa(t)\sim\frac{\langle v^2\rangle}{D_\alpha}\frac{sin(\alpha\pi)}{\alpha}t^{-\alpha},\quad\left(t\to\infty\right) \tag{43}$$

It is noted that the asymptotic behavior, $(t)\sim t^{-\alpha}\ \left(t\to\infty\right)$, can be reproduced choosing the following expression for the memory-function [113]

$$\kappa(t)=\omega_0^2M\left(\alpha,1,-t/\tau\right) \tag{44}$$

Here, *M* (*a*,*b*,*z*) denotes the *confluent hypergeometric function* [115]. The quantity ω_0 has the dimension of frequency, and τ is a time-scale. In particular, for *a* - 0, we have $\kappa(t)=\omega_0^2\theta(t)$, and then, expression (27) is recovered. For $\alpha\neq 1$, *k*(*t* behaves, at large-time, as [113]

$$\kappa(t)\sim\omega_0^2\left(t/\tau\right)^{-\alpha}/\Gamma(1-\alpha)\ ,\ \left(t\to\infty\right) \tag{45}$$

which is conform to behavior (43).

For the determination of the diffusion exponent, *a*, relation (1) will be used, which is expressed in log-log scale. This exponent is 1, for normal diffusion regime, 0, for the plateau regime, and between 0 and 1, for the subdiffusive one.

In the next section, we shall report on MD simulations of dynamic properties of the clothed oil-droplets, in particular, their stay duration in a cage, denoted as Δt_c. In a cage, a given oil-droplet is surrounded by N_c nearest neighbors (traps). As pointed out in Ref. [53], the duration Δt_c scales as: $\Delta t_c\sim\left(N_c a^2\right)^{1/\alpha}$, where *a* is the subdiffusion exponent and *a* denotes the mean-distance between traps.

Results from MD simulations

A. Simulation strategy

For the description of the dynamic properties of PEs, using MD method, the equations of motion are solved in the canonical ensemble using the Velocity Verlet Algorithm (VVA) [116], with the Thermostat of Berendsen [117], in order to keep the temperature constant. In addition, periodic boundary conditions are applied to remove the surface effects and simulate an infinite emulsion. In the following, it will be convenient to use dimensionless units, where the length unit is σ, time in units of $\tau=\sigma\sqrt{M/\varepsilon}$, where *M* is the oil-droplet mass and ε is the depth of the interaction potential, k_BT is the energy unit, and $L_0=N\times\left(6V/\pi N\right)^{1/3}$ is the box-size, where *N*

Citation: Benhamou M, El-Moudny S (2017) Review on Pickering emulsions stabilized by adsorbed nanoparticles: Structure, Thermodynamics, Cage Effect and Subdiffusion. Int J Nanomater Nanotechnol Nanomed 3(2): 057-076. DOI: http://doi.org/10.17352/2455-3492.000022

is the number of the clothed oil-droplets, and *V* is the volume of simulation box (in *periodic conditions*). MD simulations [53] where carried out with 1728 particles and the dimensionless time-step for VVA is chosen to be 0.05.

MD strategy consists of the numerical solution, step-by-step, of the classical (coupled) equations of motion of N droplets on a discrete time-scale,

$$M_i \frac{d^2 \boldsymbol{r}_i}{dt^2} = -\frac{\partial U}{\partial \boldsymbol{r}_i} \ , \ (i = 1,\ldots,N) \qquad (46)$$

Where r_i is the position of a droplet *i*, of mass *Mi*, subject to a total force, $\boldsymbol{F}_i = -\partial U / \partial \boldsymbol{r}_i$. It will be assumed that the oil-droplets have the same mass, *M*.

The analysis of the oil-droplets trajectories, produced by MD simulations, infers the type of motion that these droplets are undergoing. MSD is one of the most commonly used function for analyzing the motion of small entities (colloids, droplets,...). It is a measure of the squared-average-distance executed by the moving oil-droplets. It is defined as

$$W(t) = \frac{1}{N} \left\langle \sum_{i=1}^{N} \left[\boldsymbol{r}_i(t) - \boldsymbol{r}_i(0) \right]^2 \right\rangle \qquad (47)$$

Here, the brackets <...> denote the ensemble-average, which is the statistical average of the quantity inside the brackets, at a given time over all systems of the ensemble. Formula (9) in log-log scale allows the computation of the subdiffusion exponent, *a*, and the fractional diffusion coefficient, D_a, by extrapolation.

The second basic quantity is VACF that measures the correlations between the velocity of the oil-droplets, at times *t* = 0 and *t*. Within MD simulation scheme, VACF is defined as

$$c_{vv}(t) = \frac{1}{N} \left\langle \sum_{i=1}^{N} \left[\boldsymbol{v}_i(t) - \boldsymbol{v}_i(0) \right]^2 \right\rangle \qquad (48)$$

As we shall see below, in particular, such a function informs on the existence of the *cage effect*.

B. Charge effects

The goal of this paragraph is to quantify the influence of the charge carried by the oil-droplets on their dynamic properties. More details concerning the charge effects can be found in Ref. [53], we simply recall the essential of the study. Here, the size of the oil-droplets, their reduced number density and the salt-concentration are fixed to the values: $\sigma = 20000$ Å, $\rho^* = 0.0020$ and $c_s = 2.91\,\mu M$. But the valence, *Z*, is varied from 1000 to 4500.

Figure 8 shows the log-log plot of the reduced MSD upon dimensionless time, t/τ, for various values of the surface charge. First, remark that, for short-times, the curves for different surface charges are superposed, and then, the tracer follows a normal diffusion, that is $W(t) = 6Dt$, for times less than a *reduced transition time*, $t_1 \simeq 2.483$. The (reduced) normal diffusion coefficient is $D \simeq 14.120$, independently of the values of the surface charge. This normal behavior is synonym of the absence of the correlations between the oil-droplets, at intermediate times, whatever are the values of their surface charge. We recall that such a regime has been already observed in some work by Tata and *coworkers* [118] on colloidal suspensions using the Brownian Dynamics simulation [116]. Then, the simulated normal regime agrees well with the predicted theoretical formula (20).

Remark that the normal diffusion is followed by a transient plateau-like regime, before a subdiffusion takes place. As shown in Figure 8, the plateau is more and more pronounced, for higher surface charges. We note that the existence of this plateau regime is conform with the theoretical equation (38).

For large-times, however, the situation is quite different and the dynamic of the oil-droplets depends heavily on their surface charge, and one assists to a formation of cages, where a given charged oil-droplet is surrounded by their nearest neighbors. Also, remark that the crossover time, $t_2 > t_1$, between the plateau-like regime and the subdiffusion depends on the value of the surface charge. In this large-time regime, MSD behaves rather as $W(t) \sim D_\alpha t^\alpha$, with an average subdiffusion exponent $\alpha_c = 0.418$.

As already shown [53], the stay duration in a cage of a given moving oil-droplet, denoted as $\Delta t_c = t_2 - t_1$, increases with increasing surface charge. This tells us that the moving oil-droplet needs more time to break free of the cage of its nearest neighbors, as the surface charge increases. Physically speaking, for higher surface charges, the available space for the oil-droplets becomes effectively reduced by the volume-excluding, due to a strong repulsion force between them. Then, one assists to a slowing down of the diffusion process of the oil-droplets, which stay localized for some time that increases with increasing surface charge. Such a behavior is also reflected in VACFs displayed in figure 9, for the same values of the surface charge. VACFs are characterized by an underdamped (oscillatory) decay, more pronounced, for higher surface charges, in perfect agreement with the predicted theoretical formula (31). In fact, this underdamped feature can be related to the confinement of the random walker in the cage formed by its nearest neighbors [113], and means that the diffusion process is not Markovian, but rather has memory [111]. For low-surface charges, as can be seen in this figure,

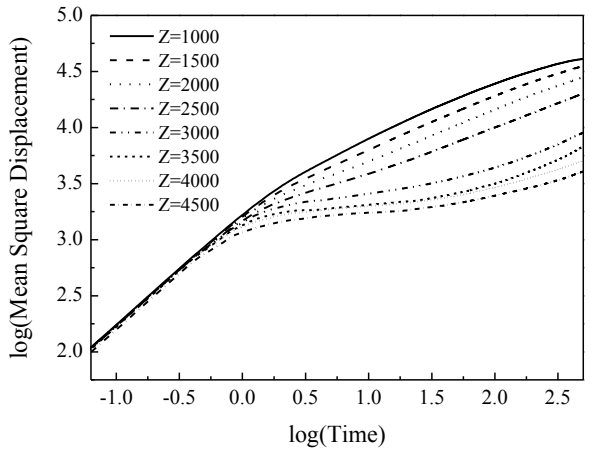

Figure 8: MSD versus the dimensionless time, t / τ, in log-log scale, for various values of the oil-droplet surface charge, with the fixed parameters: σ = 20000 Å, ρ^* = 0.0020 and c_s = 2.91 μM.

Citation: Benhamou M, El-Moudny S (2017) Review on Pickering emulsions stabilized by adsorbed nanoparticles: Structure, Thermodynamics, Cage Effect and Subdiffusion. Int J Nanomater Nanotechnol Nanomed 3(2): 057-076. DOI: http://doi.org/10.17352/2455-3492.000022

VACF is rather an overdamped function, as predicted by the theoretical expression (32). Also, observe that, for any value of the surface charge, the tail or the long-time behavior of VACFs, which reflects the diffusional regime of the oil-droplets under consideration, approaches asymptotically zero, from negative values. Therefore, the oil-droplets display a subdiffusion. This negative region indicates that, on average, a displacement of the oil-droplets surrounded by its nearest neighbors is followed by a displacement back toward its initial position (non-vanishing survival probability) [113]. In other words, this reflects the fact that the velocity of the oil-droplets is, on average, reversed by repulsion with the cage made of nearest neighbors.

As already shown [53], both anomalous diffusion exponent, α , and fractional diffusion coefficient, D_a, decrease progressively with the surface charge. As the later is augmented, the correlations between the oil-droplets become stronger, and consequently, one assists to a slow dynamic.

Also, it was pointed out [53] that the charge-behavior of the fractional diffusion coefficient can be described using an *Arrhenius*' law [53], that is $D_\alpha = D_0 exp\left\{-\left(Z/Z^*\right)^2\right\}$, with known amplitude, D_0, and range, Z^*, which are *not* universal, but they mainly depend on the other remaining factors (density, salt-concentration).

C. Density effects

Now, we report on the study of the influence of the density of the clothed oil-droplets on their dynamics [53], fixing their surface charge and size, and the salt-concentration to the values: $Z = 2000$, $\sigma = 20000$ Å, and $c_s = 2.91\,\mu M$.

Figure 10 shows the log-log plot of MSD, versus the dimensionless time, t/τ, for various values of the droplet-density. First, remark that for $t < t'_1$, with $t'_1 = 1.449$ (*second reduced transition time*), MSDs present as straight lines having the same slope, but decrease, as the oil-droplet density is increased. This time-behavior agrees well with the predicted theoretical formula (20). Therefore, the tracer executes a normal Brownian diffusion, whose MSD is $W(t) = 6D(\rho)t$, for $t < t'_1$. Here, $D(\rho) = k_B T / 6\pi\eta(\rho)R$ accounts for the usual diffusion coefficient, where *R* is the droplet-radius and $\eta(\rho)$ is the density-dependent viscosity, relation (11). As demonstrated by MD simulations [53], this same coefficient decreases with increasing density. Second, for $t > t'_1$, a cage effect is observed, where MSDs are very sensitive to the variation of the oil-droplet density, and exhibit a subdiffusive behavior, with an average subdiffusion exponent, $\alpha_d = 0.432$. The existence of such a regime is conform with the predicted theoretical formula (39).

It was also observed [53] that, as it $\Delta t'_c$ should be, the stay duration of the random walker in a cage, , increases with increasing droplet-density.

The subdiffusive behavior we evoked above is shown in figure 11, which represents the variation of VACFs versus the reduced time, t/τ , for different values of the droplet-density. These plots clearly show that the negative region of VACFs becomes more larger, by a progressive increase of the droplet-density. In particular, it was observed that VACF is underdamped

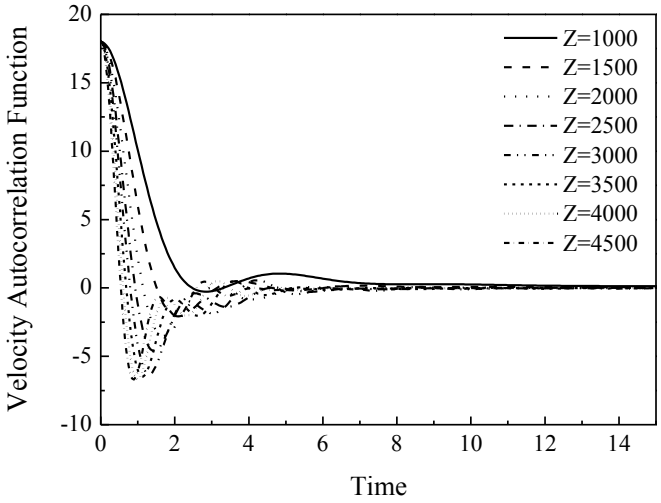

Figure 9: VACF versus the dimensionless time, t/τ, for various values of the oil-droplet surface charge, with the fixed parameters: σ = 20000 Å, ρ^* = 0.0020 and c_s = 2.91 μ*M*.

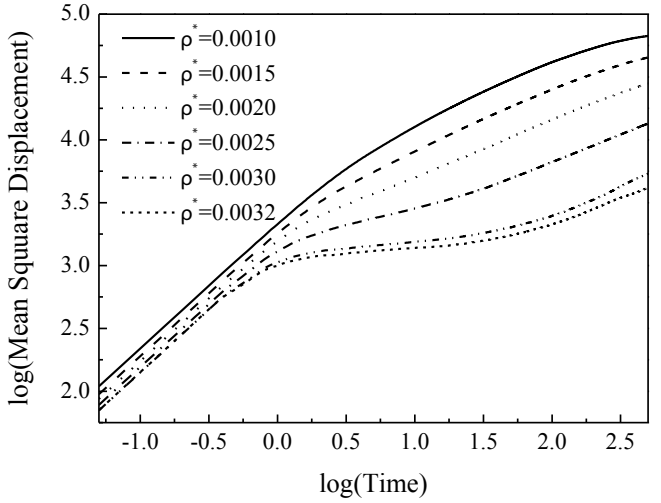

Figure 10: MSD versus the dimensionless time, t/τ, in log-log scale, for various values of the oil-droplet density, with the fixed parameters: Z = 2000, σ = 20000 Å, and c_s = 2.91 μ*M*.

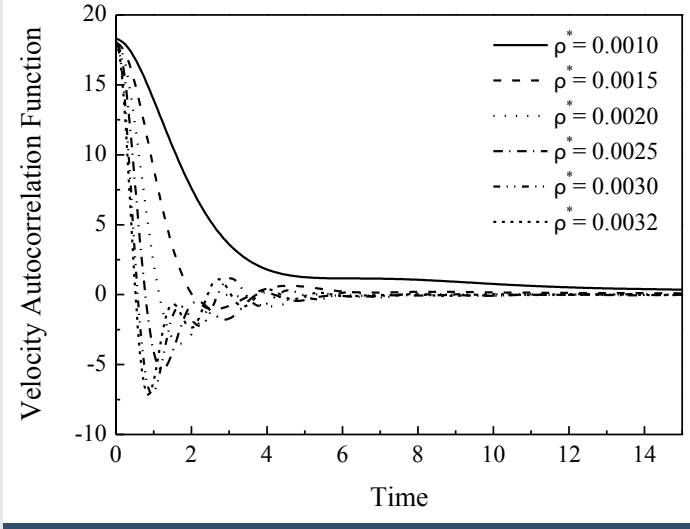

Figure 11: VACF versus the dimensionless time, t/τ, for various values of the oil-droplet density, with fixed parameters: Z = 2000, σ = 20000 Å, and c_s = 2.91 μ*M*.

Citation: Benhamou M, El-Moudny S (2017) Review on Pickering emulsions stabilized by adsorbed nanoparticles: Structure, Thermodynamics, Cage Effect and Subdiffusion. Int J Nanomater Nanotechnol Nanomed 3(2): 057-076. DOI: http://doi.org/10.17352/2455-3492.000022

(oscillatory), for high-densities, and overdamped, for low-densities. This is in perfect agreement with the theoretical formulae (31) and (32), respectively. In addition, these plots show that VACFs tails approach asymptotically zero, from negative values. This means that the oil-droplets undergo a subdiffusion, with a subdiffusion exponent, *a*, in the interval $0 < \alpha < 1$.

On the other side, MD data [53] indicate that the subdiffusion exponent, *a*, and the corresponding fractional diffusion constant, D_a, decrease progressively, as the droplet-density is augmented. This tendency is due to the strong correlations between the droplets, in high-density regime.

Finally, as already shown [53], the behavior of the fractional diffusion coefficient can also be modelled by a law of *Arrhenius* type, that is $D_\alpha = D'_0 \, exp\{-\rho / \rho_0\}$, with known amplitude, D'_0, and range, ρ_0. Naturally, these quantities are *not* universal, but mainly depend on the values of the other pertinent factors (surface charge, salt-concentration).

D. Salt-concentration effects

In this paragraph, we report on a quantitative investigation of the effects of the salt-concentration. c_s, on the oil-droplets dynamics, fixing the remaining parameters to the values: $Z = 500$, $\sigma = 5000$ Å, and $\rho^* = 0.0020$.

Figure 12 shows the log-log plot of MSD, versus the dimensionless time, t / τ, for several values of the salt-concentration. First, observe that, for $t < t''_1$, with $t''_1 = 1.439$ (*third reduced transition time*), MSDs increase linearly with time, and have practically the same slope, whatever is the value of the salt-concentration. This indicates that the random walker follows a normal Brownian diffusion, whose MSD is $W(t) = 6Dt$, for $t < t''_1$, with the (reduced) normal diffusion coefficient $D = 14.186$. As noted [53], such a time-behavior agrees well with the theoretical formula (20).

Second, for large-times $(t > t''_1)$, as observed by MD simulations [53], MSDs become very sensitive to the variation of the salt-concentration, and then, they present a subdiffusive behavior, due to a cage effect, with an average subdiffusion exponent, $\alpha_s = 0.467$. Before this regime is reached, MSDs exhibit a plateau, which is pronounced, only for low-salt-concentrations. The existence of such a regime is in perfect agreement with the theoretical formula (39).

Figure 13 represents VACFs, versus the reduced time, t / τ, for various values of the salt-concentration. These curves show that VACFs are underdamped (oscillatory), for low-salt-concentrations, and overdamped (non-oscillatory), for high-salt-concentrations, before they reach a negative region that becomes more and more pronounced, as the salt-concentration is decreased. Emphasize that the existence of the underdamped and overdamped behaviors agree with the theoretical formulae (31) and (32). Therefore, the cage effect is more significant, and the stay duration of a random walker in a cage, $\Delta t''_c$, decreases

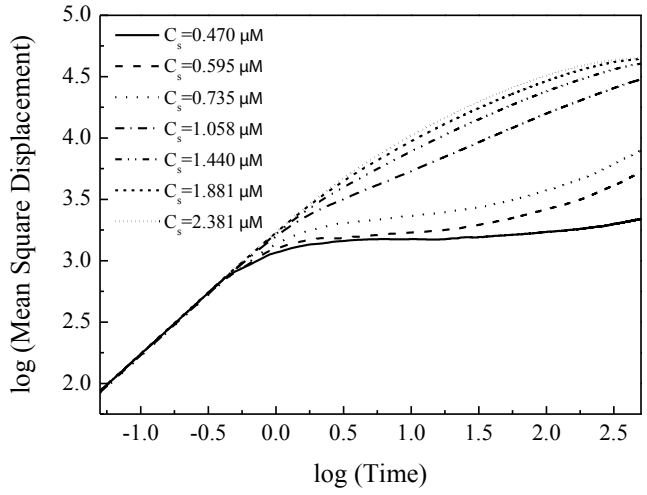

Figure 12: MSD versus the dimensionless time, t / τ, in log-log scale, for various values of the salt-concentration, with fixed parameters: Z = 500, σ = 5000 Å, and ρ* = 0.0020.

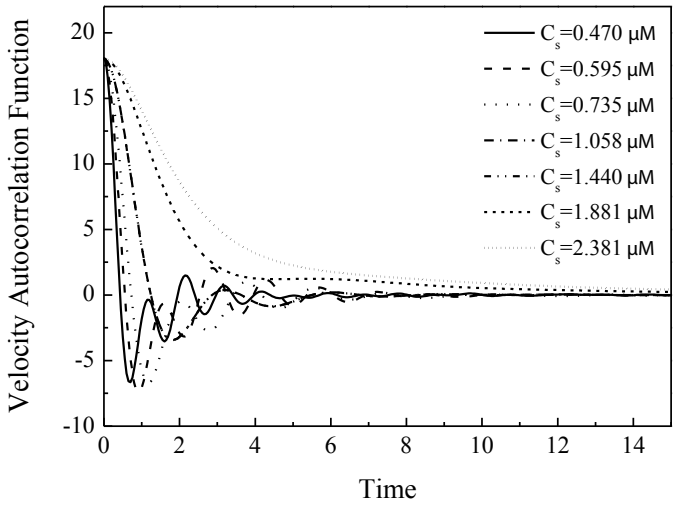

Figure 13: VACF versus the dimensionless time, t / τ, for different values of the salt-concentration, with fixed parameters: Z = 500, σ = 5000 Å, and ρ* = 0.0020.

with increasing salt-concentration. In fact, this is due to a drastic diminishment of the strength of the mutual interactions between charged oil-droplets. Also, these curves indicate that VACFs tails reach asymptotically zero, from negative values. This is a signature of the existence of a subdiffusion regime, with an anomalous diffusion exponent, *a*, between 0 and 1.

In addition, it was numerically observed [53] that the subdiffusion exponent, *a*, and the associated fractional diffusion coefficient, D_a, increase progressively, as the salt-concentration is augmented. Then, by an increase of this concentration, the diffusion becomes less slower, due to the weak correlations between the random walkers.

Finally, as reported in Ref. [53], the behavior of the fractional diffusion coefficient can be approached by a shifted *Arrhenius* law, that is $D_\alpha = D_1 + D_2 exp\{-c_s / c_s^*\}$, with known quantities D_1,D_2 and c_s^*, which naturally depend on the other pertinent factors (density, surface charge).

Citation: Benhamou M, El-Moudny S (2017) Review on Pickering emulsions stabilized by adsorbed nanoparticles: Structure, Thermodynamics, Cage Effect and Subdiffusion. Int J Nanomater Nanotechnol Nanomed 3(2): 057-076. DOI: http://doi.org/10.17352/2455-3492.000022

Spherical diffusion of anchored nanoparticles

Introduction : Consider a PE of O/W type, where the oil-droplets are covered by strongly adsorbed charged nanoparticles that ensures their stabilization. The adsorption energy is high enough, in comparison with the thermal energy, $k_B T$. Then, the presence of the charge carried by the droplets prevent the coalescence phenomenon, when two neighboring droplets touch.

Diffusion on a curved surface, like a sphere, is a major problem that arises in several contexts. For example, the diffusion is an important mode of transport of biological substances (lipids and proteins) on the cell walls, which are curved surfaces. Spherical diffusion also crops up in surface smoothening in computer graphics and global migration patterns of marine mammals. While planar diffusion has been studied extensively both analytically and numerically, but there have been fewer analytical studies of diffusion on spherical surfaces.

In a very recent work [55], using PEs as templates, the authors have established the diffusion laws of the anchored nanoparticles undergoing Brownian motion on the surface of droplets.

The aim is an investigation of the spherical diffusion laws of the adsorbed charged nanoparticles, using some theory based on the Green's function techniques.

Theoretical formulation : In this paragraph, the aim is the determination of the Green's function allowing the derivation of the surface diffusion laws. As we shall see below, such a function solves the spherical diffusion equation.

When modelling the diffusion phenomena in an infinite medium, one often solves the diffusion equation for the probability density, $u(x,t)$, subject to a given initial condition: $u(x,0)=f(x)$, where $f(x)$ is a regular distribution (*Cauchy condition*). Here, *x* denotes the space coordinate and is the time-variable.

A one-dimensional linear diffusion equation, with constant diffusion coefficient, is defined as [119]

$$\frac{\partial u}{\partial t} = D\Delta u \tag{49}$$

Where *D* is the diffusion coefficient, and Δ represents the Laplace operator.

The spherical diffusion equation reads

$$\frac{\partial u(\theta,\phi,t)}{\partial t} = k\Delta_{S^2} u(\theta,\phi,t) \tag{50}$$

with the notation: $k = D/R^2$, where *R* accounts for the droplet-radius. Here, $\Delta_{(S^2)}$ denotes the spherical Laplace operator, called *Laplace-Bertlami* operator. Its expression is

$$\Delta_{S^2} = \frac{1}{\sin}\frac{\partial}{\partial\theta}(\sin\theta\frac{\partial}{\partial\theta}) + \frac{1}{\sin^2\theta}\frac{\partial^2}{\partial\phi^2} \tag{51}$$

In obtaining the solutions to Laplace's equation in spherical coordinates, it is traditional to introduce the *spherical harmonics*, $Y_l^m(\theta,\phi)$. These special functions are defined by [115].

$$Y_l^m(\theta,\phi) = N_{lm} P_l^m(cos\theta) e^{im\phi} \tag{52}$$

with the normalization constant

$$N_{lm} = \sqrt{\left(\frac{2l+1}{4\pi}\right)\left(\frac{l-m}{l+m}\right)} \tag{53}$$

and the associated *Legendre functions*

$$P_l^m(x) = \frac{(-1)^m(1-x)^{m/2}}{2^l l!} \times \frac{d^{l+m}}{dx^{l+m}}\left(x^2-1\right)^l \tag{54}$$

We note that the normalization factor, N_{lm} , has been chosen such that the spherical harmonics are normalized to 1.

For solving the diffusion equation, use is made of the usual separation of variables

$$u_{lm}(\theta,\phi,t) = Y_l^m(\theta,\phi)T(t) \tag{55}$$

Inserting this decomposition into the spherical diffusion equation (50), and using the fact that the spherical harmonics are eigenfunctions of the spherical Laplace operator yield

$$u_{lm}(\theta,\phi,t) = Y_l^m(\theta,\phi)e^{-l(l+1)kt} \tag{56}$$

Now, to derive the expression of the Green's function, the following initial condition is imposed

$$u_{lm}(\theta,\phi,0) = \delta_{S^2}(\theta,\phi) \tag{57}$$

where symbol $\delta_{S^2}(\theta,\phi)$ denotes la spherical Dirac distribution, defined by [119]

$$\delta_{S^2}(\theta,\phi) = \sum_{l\in N}\left(\frac{2l+1}{4\pi}\right)P_l(cos\theta) \tag{58}$$

Therefore, the final expression of the Green's function is

$$G(\theta,\phi,t) = \sum_{l\in N}\sqrt{\frac{2l+1}{4\pi}}u_{l0}(\theta,\phi,t) \tag{59}$$

with

$$u_{l0}(\theta,\phi,t) = Y_l^0(\theta,\phi)e^{-l(l+1)kt} \quad , \quad k = D/R^2 \tag{60}$$

Results and Discussion

The statistical properties of the anchored nanoparticles can be described by the Green's function (propagator) $G(\boldsymbol{r},t) = G(\theta,\phi,t)$. The latter represents the probability to find an anchored nanoparticle (random walker) at position *r*, at time *t*, with the initial condition: $G(\boldsymbol{r},0) = \delta_2(\boldsymbol{r})$, where δ_2 is the two-dimensional Dirac distribution.

Once the Green's function is known, all the statistical properties can be computed. For instance, MSD can be obtained from

$$\langle r^2(t)\rangle = R^2 \sum_{l\in N}(2l+1)e^{-l(l+1)kt}\int_0^\pi d\theta sin\theta(1-cos\theta)P_l(cos\theta) \tag{61}$$

where $\tau = R^2/D$ denotes the relaxation time, and *R* is the droplet-radius.

From the well-known results of integrals [115], one finds

$$\langle r^2(t)\rangle = 2R^2\left(1-e^{-2t/\tau}\right). \tag{62}$$

Citation: Benhamou M, El-Moudny S (2017) Review on Pickering emulsions stabilized by adsorbed nanoparticles: Structure, Thermodynamics, Cage Effect and Subdiffusion. Int J Nanomater Nanotechnol Nanomed 3(2): 057-076. DOI: http://doi.org/10.17352/2455-3492.000022

As expected, MSD saturates to $\langle r^2(t)\rangle = 2R^2$, , for large-times, that is for $t >> \tau$. For short-times $(t \ll \tau)$, however, MSD does not depend on the radius of the sphere, and the celebrated (planar) Einstein's diffusion law is then recovered. This result can be explained by the fact that, in short-time limit, the anchored nanoparticle has not enough time to feel the influence of the curvature of the spherical surface of the dispersed droplets.

To sum up, we recall that, in this paragraph, we have reported on the diffusion of confined nanoparticles on a sphere, using PEs as templates. In particular, as we noted above, for short-times, the nanoparticle does not feel the influence of the droplet-shape.

Conclusion

This survey focuses on physics of PEs of O/W type, which are stabilized by a strong irreversible adsorption of charged nanoparticles on the surface of the dispersed oil-droplets. The adsorption energy is very high, compared to the thermal energy, k_BT. As consequence, on one hand, this special process prevents the coalescence phenomenon leading to a complete separation between oil and water, and on the other hand, it ensures a long-time stabilization of these emulsions, in comparison with the standard way that consists in using surfactant molecules.

For the study, PEs was regarded as colloidal solutions, where the clothed oil-droplets play the role of soft-colloids. For the sake of simplicity, the anchored nanoparticles were assumed to be point-like. In fact, such an assumption makes sense only when their size is much smaller than the droplet-diameter, and in addition, when one is concerned with phenomena occurring at large-scale (distance, wavelength...). Particles shape and form are pertinent regarding their diffusion on the droplets surfaces. Also, it was supposed that the anchored nanoparticles are uniformly distributed on the O/W interfaces, but as pointed out in some recent experiment [7], these nanoparticles may be aggregated due to a depletion force, contrarily to charged solid colloids (latex polyballs, for example). Then, the presence of strong charges on O/W interfaces prevents such an aggregation.

Emphasize that an adsorption of charged nanoparticles on the interfaces between two incompatible liquids is not the only way to stabilize PEs. For instance, an alternative method consist in adding a diblock-copolymer formed by two unlike-chains (PS/PVME, for example), each is soluble in one liquid, only. The droplets can be regarded as star-polymers, and then, the floating chains ensure their stabilization, due to the excluded volume forces between monomers. Such a question is of interest, due to the fact that this stabilization mechanism may be very useful for the elaboration of new nanocomposites, for industrial purposes.

We reported on three important points: (1) Structure and thermodynamics of PEs of O/W type, from a static point of view, using the integral equation approach, (2) some dynamic aspect in relation with the cage effect and subdiffusion within these emulsions, and (3) spherical diffusion of the anchored nanoparticles on the (curved) water/oil interface.

For the study of the structure and thermodynamics of PEs, the adopted pair-potential between the clothed oil-droplets is that of Sogami-Ise. The virtues of this potential are that, first, it reproduces the features of the real potential, since it is the sum of a repulsive part and an attractive one, and second, it was a good candidate for the explanation of many experimental measurements, in the past.

The computed quantities are the structure-factor and the spatial correlation-function, from which were extracted the thermodynamical properties, as pressure, internal energy and thermal compressibility. Discussion was done, in terms of the essential factors governing physics, as the density of the oil-droplets, their size and surface charge, and the salt-concentration. In the same context, a successful comparison [48] between results from integral equation method and MD simulations has shown their good agreement.

The second raised point is how the stabilization process is accomplished in time. MD simulations [53], with Sogami-Ise potential, has been used to investigate quantitatively this dynamic process, and it has been shown that the clothed oil-droplets execute rather a slow diffusion motion (subdiffusion), due to the complex structure of PEs leading to a cage effect, contrarily to the diffusion in the homogeneous media. A random walker (a given clothed oil-droplet) is then subject to a subdiffusion characterized by an anomalous diffusion exponent, α, between 0 and 1. Of course, this exponent is not a universal quantity but, as observed [53], it mainly depends on the pertinent factors cited above. In particular, it was found [53] that the subdiffusion process is pronounced only for high surface charges and densities, and low salt-concentration. But for experimentalists, the good way is to vary rather the salt-concentration (keeping fixed the other parameters), in order to control well the diffusion phenomenon.

To validate MD simulations data, the authors have proposed a memory diffusion theory, based essentially on a generalized Langevin equation. Physics was studied through the evolutions of MSD and VACF in time. It was observed [53] that the results from simulations agree well with the theoretical predictions.

It is noted that the added nanoparticles stabilizing the emulsion are abundant, and only some of them are adsorbed onto the O/W interfaces. The remaining nanoparticles are dissociated in water in form of coions, and then contribute to an increase of the salt-concentration coming from the counter-ions and the added salt. The subdiffusion process is then disadvantaged by the presence of an excess of the added nanoparticles.

Underline that we have not discussed the effect of the size of the clothed oil-droplets on their dynamic properties. In fact, this size is controlled by the number of charged nanoparticles anchored on the surfaces of the oil-droplets, which approximately equals their valence, Z. As observed experimentally [3], the droplet-size decreases with the valence Z. Therefore, small sizes correspond to strong surface charges. Consequently, the subdiffusion process is more pronounced, only for droplets of small-size.

Citation: Benhamou M, El-Moudny S (2017) Review on Pickering emulsions stabilized by adsorbed nanoparticles: Structure, Thermodynamics, Cage Effect and Subdiffusion. Int J Nanomater Nanotechnol Nanomed 3(2): 057-076. DOI: http://doi.org/10.17352/2455-3492.000022

We point out that the present study may be extended to PEs that are composed of two incompatible polymers trapped in a common good solvent (water, for instance). There kinds of emulsions are called "water-in-water solutions" in the literature [7].

The last discussed point is an exact study of the spherical diffusion of the confined nanoparticles on the spherical surface of droplets. In particular, it was found [55] that, for short-times, the diffusion of a given nanoparticle (tracer) does not feel the influence of the droplet-shape, and this diffusion remain normal.

Finally, it will be interesting to extend these extensive studies to the situation where the anchored nanoparticles have arbitrary shapes and forms (rods, ellipsoids, polyelectrolytes...).

Acknowledgments

We are much indebted to Professors D. Durand and L. Benyahia for helpful discussions. One of us (M.B.) would like to thank *Le Mans University* for their kind of hospitality during his regular visits. We are very grateful to our referee for its pertinent remarks and useful suggestions.

References

1. W Ramsden (1903) Separation of solids in the surface layers of solutions and suspensions. Proc Royal Soc (London) 72: 156-164. Link: https://goo.gl/WKoCJk

2. SU Pickering (1907) Cxcvi.-Emulsions. J Chem Soc Transactions 91: 2001-2021. Link: https://goo.gl/8TQfhc

3. R Aveyard, BP Binks, JH Clint (2003) Emulsions stabilized solely by solid colloidal particles. Adv Coll Inter Sci 100-102: 503-546. Link: https://goo.gl/QYmv5P

4. BP Binks (2002) Particles as surfactants-similarities and differences. Curr Opin Coll Inter Sci 7: 21-41. Link: https://goo.gl/PvMXzP

5. BP Binks, TS Horozov (2006) Colloidal Particles at Liquid Interfaces. Cambridge University Press. Link: https://goo.gl/WyLPn9

6. Y Chevalier, MA Bolzinger (2013) Emulsions stabilized with solid nanoparticles: Pickering emulsions. Coll. Surf. A: Physicochemical and Engineering Aspects 439: 23-34. Link: https://goo.gl/ZZx4xx

7. G Balakrishnan, T Nicolai, L Benyahia, D Durand (2012) Particles trapped at the droplet interface in water-in-water emulsions. Langmuir 28: 5921-5926; also, BT Nguyen T Nicolai, L Benyahia (2013) Stabilization of water-in-water emulsions by addition of protein particles. Langmuir 23: 1453-1458. Link: https://goo.gl/ML1h5r Link: https://goo.gl/hGyNcy

8. NP Pardhy, BM Budhlall (2010) Pickering emulsion as a template to synthesize Janus colloids with anisotropy in the surface potential. Langmuir 26: 13130-13141. Link: https://goo.gl/HW5nbm

9. JH Chen, CY Cheng, WY Chiu, CF Lee, NY Liang (2008) Synthesis of ZnO/polystyrene composites particles by Pickering emulsion polymerization. Eur Polym J 44: 3271-3279. Link: https://goo.gl/P9hTzA

10. PJ Colver, CA Colard, SA Bon (2008) Multilayered nanocomposite polymer colloids using emulsion polymerization stabilized by solid particles. J Am Chem Soc 130: 16850-16851. Link: https://goo.gl/n67Qoa

11. C Wang, C Zhang, Y Li, Y Chen, Z Tong (2009) Facile fabrication of nanocomposite microspheres with polymer cores and magnetic shells by Pickering suspension polymerization. Reactive and Functional Polymers 69: 750-754. Link: https://goo.gl/4pCAkH

12. K Zhang, W Wu, H Meng, K Guo, JF Chen (2009) Pickering emulsion polymerization: Preparation of polystyrene/nano-SiO composite microspheres with core-shell structure. Powder Technology 190: 393-400. Link: https://goo.gl/nNKxPh

13. H Ma, M Luo, S Sanyal, K Rege, LL.Dai (2010) The one-step Pickering emulsion polymerization route for synthesizing organic-inorganic nanocomposite particles. Materials 3: 1186-1202. Link: https://goo.gl/Fr5wdx

14. G Yin, Z Zheng, H Wang, Q Du (2011) Slightly surface-functionalized polystyrene microspheres prepared via Pickering emulsion polymerization using for electrophoretic displays. J Coll Inter Sci 361: 456-464. Link: https://goo.gl/9RQghX

15. M Zhang, TH Ngo, NI Rabiah, TP Otanicar, PE Phelan, et al. (2013) Core-shell and asymmetric polystyrene-gold composite particles via one-step Pickering emulsion polymerization. Langmuir 30: 75-82. Link: https://goo.gl/fmKiqm

16. L Hao, C Wang, Z Tong (2013) Nanocomposite polysaccharide microcapsules fabricated through layer-by-layer assembly based on a Pickering emulsion template. Journal of Controlled Release 172: 19-139. Link: https://goo.gl/J4tW63

17. AK Dyab, HA Al-Lohedan, HA Essawy, AIA El-Mageed, F Taha (2014) Fabrication of core/shell hybrid organic-inorganic polymer microspheres via Pickering emulsion polymerization using laponite nanoparticles. J Saudi Chem Soc 18: 610-617. Link: https://goo.gl/3cGcss

18. J Ji, S Shu, F Wang, Z Li, J Liu, et al. (2014) Core-shell-structured silica/polyacrylate particles prepared by Pickering emulsion: Influence of the nucleation model on particle interfacial organization and emulsion stability. Nanoscale Research Letters 9: 1-9. Link: https://goo.gl/RA2YSM

19. AD Dinsmore, MF Hsu, MG Nikolaides, M Marquez, AR Bausch, et al. (2002) Colloidosomes: Selectively permeable capsules composed of colloidal particles. Science 298: 1006-1009. Link: https://goo.gl/QQ2WfG

20. T Chen, PJ Colver, SA Bon (2007) Organic-inorganic hybrid hollow spheres prepared from TiO-stabilized Pickering emulsion polymerization. Advanced Materials 19: 2286-2289. Link: https://goo.gl/mLn31J

21. W Chen, X Liu, Y Liu, HI Kim (2010) Synthesis of microcapsules with polystyrene/ZnO hybrid shell by Pickering emulsion polymerization. Coll Polym Sci 288: 1393-1399. Link: https://goo.gl/t218xX

22. BP Binks, SO Lumsdon (2000) Influence of particle wettability on the type and stability of surfactant-free emulsions. Langmuir 16: 8622-8631. Link: https://goo.gl/gdoRY5

23. D Rousseau (2000) Fat crystals and emulsion stability-a review, Food Research International 33: 3-14. Link: https://goo.gl/2PEF8B

24. BP Binks, JH Clint (2002) Solid wettability from surface energy components: Relevance to Pickering emulsions. Langmuir 18: 1270-1273. Link: https://goo.gl/iFcbyM

25. MJ Hey, JG Kingston (2006) Maximum stability of a single spherical particle attached to an emulsion drop. J Coll Inter Sci 298: 497-499. Link: https://goo.gl/yuitZv

26. VN Paunov, OJ Cayre, PF Noble, SD Stoyanov, KP Velikov, et al. (2007) Emulsions stabilised by food colloid particles: Role of particle adsorption and wettability at the liquid interface. J Coll Inter Sci 312: 381-389. Link: https://goo.gl/p35ENb

27. S Sacanna, WK Kegel, AP Philipse (2007) Thermodynamically stable Pickering emulsions. Phys Rev Lett 98: 158301-158305. Link: https://goo.gl/WZxNRj

28. J Frelichowska, MA Bolzinger, Y Chevalier (2009) Pickering emulsions with bare silica. Coll Surf A: Physicochemical and Engineering Aspects 343: 70-74. Link: https://goo.gl/yexRkL

Citation: Benhamou M, El-Moudny S (2017) Review on Pickering emulsions stabilized by adsorbed nanoparticles: Structure, Thermodynamics, Cage Effect and Subdiffusion. Int J Nanomater Nanotechnol Nanomed 3(2): 057-076. DOI: http://doi.org/10.17352/2455-3492.000022

29. R Aveyard (2012) Can Janus particles give thermodynamically stable Pickering emulsions? Soft Matter 8: 5233-5240. Link: https://goo.gl/eAhVh6

30. M Rayner, D Marku, M Eriksson, M Sjöö, P Dejmek, et al. (2014) Biomass-based particles for the formulation of Pickering type emulsions in food and topical applications. Coll Surf A: Physicochemical and Engineering Aspects 458: 48-62. Link: https://goo.gl/en5Ds1

31. BP Binks, W Liu, JA Rodrigues (2008) Novel stabilization of emulsions via the heteroaggregation of nanoparticles Langmuir 24: 4443-4446. Link: https://goo.gl/PZqtuH

32. TLiu, S Seiffert, J Thiele, AR Abate, DA Weitz, et al. (2012) Non-coalescence of oppositely charged droplets in pH-sensitive emulsions. Proceedings of the National Academy of Sciences 109: 384-389. Link: https://goo.gl/upb8mn

33. H Wang, V Singh, SH Behrens (2012) Image charge effects on the formation of pickering emulsions. J Phys Chem Lett 3: 2986-2990. Link: https://goo.gl/ZJxRov

34. T Nallamilli, E Mani, MG Basavaraj (2014) A model for the prediction of droplet size in Pickering emulsions stabilized by oppositely charged particles. Langmuir 30: 9336-9345. Link: https://goo.gl/3mY9jF

35. NP Ashby, BP Binks (2000) Pickering emulsions stabilised by laponite clay particles. Phys Chem Chem Phys 2: 5640-5646. Link: https://goo.gl/dtywqT

36. BP Binks, SO Lumsdon (2001) Pickering emulsions stabilized by monodisperse latex particles: Effects of particle size. Langmuir 17: 4540-4547. Link: https://goo.gl/TbQfh2

37. JI Amalvy, SP Armes, BP Binks, JA Rodrigues, GF Unali (2003) Use of sterically-stabilised polystyrene latex particles as a pH-responsive particulate emulsifier to prepare surfactant-free oil-in-water emulsions. Chem Comm 15: 1826-1827. Link: https://goo.gl/dkP4rx

38. H Wang, EK Hobbie (2003) Amphiphobic carbon nanotubes as macroemulsion surfactants. Langmuir 19: 3091-3093. Link: https://goo.gl/axh9h3

39. LS Dorobantu, AK Yeung, JM Foght, MR Gray (2004) Stabilization of oil-water emulsions by hydrophobic bacteria. Applied and Environmental Microbiology 70: 6333-6336. Link: https://goo.gl/pjyHQw

40. F Gautier, M Destribats, R Perrier-Cornet, JF Dechézelles, J Giermanska, et al. (2007) Pickering emulsions with stimulable particles: From highly- to weakly-covered interfaces. Phys Chem Chem Phys 9: 6455-6462. Link: https://goo.gl/oa6RTh

41. DE Tambe, MM Sharma (1993) Factors controlling the stability of colloid-stabilized emulsions: I. An experimental investigation. J Coll Inter Sci 157: 244-253. Link: https://goo.gl/o3Bkst

42. F Yang, Q Niu, Q Lan, D Sun (2007) Effect of dispersion pH on the formation and stability of Pickering emulsions stabilized by layered double hydroxides particles. J Coll Inter Sci 306: 285-295. Link: https://goo.gl/jicgrs

43. AK Dyab (2012) Destabilisation of Pickring emulsions using pH. Coll Surf A: Physicochemical and Engineering Aspects 402: 2-12. Link: https://goo.gl/MbZR9c

44. Z Luo, BS Murray, AL Ross, MJ Povey, MR Morgan, AJ Day (2012) Effects of pH on the ability of flavonoids to act as Pickering emulsion stabilizers. Coll Surf B: Biointerfaces 92: 84-90. Link: https://goo.gl/FvSpnh

45. M Destribats, M Rouvet, C Gehin-Delval, C Schmitt, BP Binks (2016) Emulsions stabilised by whey protein microgel particles: towards food-grade Pickering emulsions. Soft Matter 10: 941-6954. Link: https://goo.gl/dwo2i1

46. C Wang, C Zhang, Y Li, Y Chen, Z Tong (2009) Facile fabrication of nanocomposite microspheres with polymer cores and magnetic shells by Pickering suspension polymerization. Reactive & Functional Polymers 69: 750-754. Link: https://goo.gl/oF5o3W

47. G Poovi, S Padmapriya, S Lakshmi (2015) Review on magnetic microsphere. Global Journal of Pharmacology 9: 296-310. Link: https://goo.gl/8YzuQg

48. S El-Moudny, M Badia, M Benhamou (2017) Structure and thermodynamics of Pickering emulsions stabilized by adsorbed charged particles. J Mol Liquids 225: 174-185. Link: https://goo.gl/7JKieZ

49. J-P Hansen, IR McDonald (2006) Theory of Simple Liquids. Third Edition Elsevier Inc. Link: https://goo.gl/h1dg9c

50. I Sogami (1983) Effective potential between charged spherical particles in dilute suspension. Phys Lett A 96: 199-203. Link: https://goo.gl/tLL1NW

51. I Sogami, N Ise (1984) On the electrostatic interaction in macroionic solutions. J Chem Phys 81: 6320-6332. Link: https://goo.gl/rNHe9t

52. BV Derjaguin (1940) On the repulsive forces between charged colloid particles and on the theory of slow coagulation and stability of lyophobe sols, Trans Faraday Soc 36: 203-215; Analysis of friction and adhesion (1940) IV. The theory of the adhesion of small particles Kolloid Z 69: 155-164; EJW Verwey, JThG Overbeek (1948) Theory of the Stability of Lyophohic Colloid. Elsevier Amsterdam. Link: https://goo.gl/PhmFwg

53. M Badia, S El-Moudny, M Benhamou, M El Ossmani (2017) Study of cage effect and subdiffusion in Pickering emulsions from Molecular Dynamics simulations. Journal of Molecular Liquids 240: 1-13. Link: https://goo.gl/CrHHkn

54. BJ Alder, TE Wainwright (1957) Phase transition for a hard sphere system. J Chem Phys 27: 1208-1209. Link: https://goo.gl/NCiyDA

55. S El-Moudny, M Badia, M Benhamou (186) Spherical Brownian diffusion of particles on liquid-liquid interfaces of Pickering emulsions. IOP Conf Series: Materials Science and Engineering 186: 1-3. Link: https://goo.gl/rZMUzU

56. JO Zoppe, RA Venditti, OJ Rojas (2012) Pickering emulsions stabilized by cellulose nanocrystals grafted with thermo-responsive polymer brushes. J Coll Inter Sci 369: 202-209. Link: https://goo.gl/2CHzrQ

57. T Saigal, H Dong, K Matyjaszewski, RD Tilton (2010) Pickering emulsions stabilized by nanoparticles with thermally responsive grafted polymer brushes. Langmuir 26: 15200-15209. Link: https://goo.gl/szMJao

58. H Guo, D Yang, M Yang, Y Gao, Y Liu, et al. (2016) Dual responsive Pickering emulsions stabilized by constructed core crosslinked polymer nanoparticles via reversible covalent bonds. Soft Matter 12: 9683-9691. Link: https://goo.gl/wuGMsb

59. KS Silmore, C Gupta, NR Washburn (2015) Tunable Pickering emulsions with polymer-grafted lignin nanoparticles. J Coll Inter Sci 466: 91-100. Link: https://goo.gl/W8ijbd

60. J Lu, W Zhou, J Chen, Y Jin, KB Walters, S Ding (2015) Pickering emulsions stabilized by palygorskite particles grafted with pH-responsive polymer brushes. RSC Adv 5: 9416-9424. Link: https://goo.gl/1ibiFq

61. Y Zhu, J Sun, C Yi, W Weia, X Liu (2016) One-step formation of multiple Pickering emulsions stabilized by self-assembled poly(dodecyl acrylate-co-acrylic acid) nanoparticles. Soft Matter 12: 7577-7584. Link: https://goo.gl/EFE15a

62. N Popadyuk, A Popadyuk, I Tarnavchyk, O Budishevska, A Kohut, et al. (2015) Synthesis of covalently cross-linked colloidosomes from peroxidized Pickering emulsions. Coatings 6: 1-14. Link: https://goo.gl/2swBSP

63. AN Semenov, J-F Joanny, AR Khokhlov (1995) Associating Polymers: Equilibrium and linear viscoelasticity, Macromolecules 28: 1066-1075. Link: https://goo.gl/yRZH5g

64. M Benhamou, H Kaidi, E-K Hachem (2017) Determination of the effective pair-potential between droplets with end-grafted polymers within Pickering emulsions versus grafting-density. solvent quality and monomer concentration, submitted for publication.

Citation: Benhamou M, El-Moudny S (2017) Review on Pickering emulsions stabilized by adsorbed nanoparticles: Structure, Thermodynamics, Cage Effect and Subdiffusion. Int J Nanomater Nanotechnol Nanomed 3(2): 057-076. DOI: http://doi.org/10.17352/2455-3492.000022

65. M Born, R Oppenheimer (1927) Quantum theory of the molecules. Ann Phys (Leipzig) 84: 457-484. Link: https://goo.gl/px9MAV

66. N Ise, T Okubo, M Sugimura, K Ito, H Nolte (1983) Ordered structure in dilute solutions of highly charged polymer lattices as studied by microscopy. I. Interparticle distance as a function of latex concentration. J Chem Phys 78: 536-540. Link: https://goo.gl/PSN3no

67. JN Israelachvili (2011) Intermolecular and Surface Forces. Revised third edition Academic Press. Link: https://goo.gl/bt4Nvu

68. BVR Tata, AK Sood, R Kesavamoorthy (1990) Structure factor of charged colloidal suspensions using Brownian-dynamics simultion: Comparison of Yukawa and Sogami pair potentials. Pramana-J Phys 34: 23-31. Link: https://goo.gl/6XwPFU

69. BVR Tata, R Kesavamoorthy, AK Sood (1987) Structure factor for a two component mixture of dilute colloidal suspensions. Mol Phys 61: 943-952. Link: https://goo.gl/HgFUqC

70. AK Arora, BVR Tata, AK Sood, R Kesavamoorthy (1988) Reentrant phase transition in charged colloidal suspensions. Phys Rev Lett 60: 2438-2441. Link: https://goo.gl/cZimq4

71. GM Kepler, S Fraden (1994) Attractive potential between confined colloids at low ionic strength. Phys Rev Lett 73: 356-360. Link: https://goo.gl/jCUVDs

72. BVR. Tata, AK Arora (1995) Comment on "Attractive potential between confined colloids at low ionic strength". Phys Rev Lett 75: 3200-3200. Link: https://goo.gl/igM3ou

73. F Reif (1965) Fundamentals of Statistical and Thermal Physics, McGraw-Hill. Link: https://goo.gl/r22FLW

74. G Zerah, J-P Hansen (1986) Self-consistent integral equations for fluid pair distribution functions: another attempt. J Chem Phys 84: 2336-2343. Link: https://goo.gl/P85Bn2

75. N Jakse, J-M Bomont, I Charpentier, J-L Bretonnet (2000) Effects of dispersion forces on the structure and thermodynamics of fluid krypton. Phys Rev E 62: 3671-3678. Link: https://goo.gl/QRS9oX

76. J-L Bretonnet, N Jakse (1986) Analysis of two integral equation for simple liquids. Phys Rev B 46: 5717-5720. Link: https://goo.gl/uEBdgq

77. S Labik, A Malijevsky, P Vonka (1985) A rapidly convergent method of solving the OZ equation. Mol Phys 56: 709-715. Link: https://goo.gl/iE3LSz

78. S Lignel (2014) Emulsions eau-dans-huile générées par un procédé microfluidique: Contribution à l'étude de la congélation de l'eau dispersée en emulsion. Doctoral Dissertation, Compiegne University. Link: https://goo.gl/T3s5A6

79. YV Kalyuzhnyi, V Vlachy (1993) Integral-equation theory for highly asymmetric electrolyte solutions. Chem Phys Lett 215: 518-522. Link: https://goo.gl/9nkedt

80. YV Kalyuzhnyi, V Vlachy, MF Holovko, G Stell (1995) Multidensity integral equation theory for highly asymmetric electrolyte solutions. J Chem Phys 102: 5770-5780. Link: https://goo.gl/AkPhmH

81. B Hribar, YV Kalyuzhnyi, V. Vlachy, (1996) Ion-ion correlations in highly asymmetrical electrolytes. Mol Phys 87: 1317-1331. Link: https://goo.gl/ctqrqK

82. P Udaykumar, T Khanna, RN Behera (2013) Equilibrium structure and properties of model colloidal suspensions. Research Journal of Recent Sciences 2: 61-66.

83. P Linse (2000) Structure, phase stability, and thermodynamics in charged colloidal solutions. J Chem Phys 113: 4359-4373. Link: https://goo.gl/2g8TjL

84. A Blumen, J Klafter, G Zumofen, in Optical Spectroscopy of Glasses, edited by I. Zschokke, Reidel, Dordrecht, 1986.

85. S Havlin, D Ben-Avraham (1987) Diffusion in disordered media. Adv Phys 36: 187-292. Link: https://goo.gl/E6heSB

86. J-P Bouchaud, A Georges (1990) Anomalous diffusion in disordered media: Statistical Mechanisms, models and physical applications. Phys Rep 195: 127-293. Link: https://goo.gl/46Q5mH

87. D Nualart (2006) Fractional Brownian Motion: Stochastic Calculus and Applications, Proceedings of the International Congress of Mathematicians, edited by European Mathematical Society, Madrid, Spain.

88. S Stachura, GR Kneller (2014) Anomalous lateral diffusion in lipid bilayers observed by molecular dynamics simulations with atomistic and coarse-gained force fields, Molecular Simulation 40: 245-250. Link: https://goo.gl/JGSSGN

89. H Scher, M Lax (1973) Stochastic transport in a disordered solid. I. Theory. Phys Rev B 7: 4491-4502; (1973) Stochastic transport in a disordered solid. II. Impurity conduction. Phys Rev B 7: 4502-4519; H Scher, E Montroll (1975) Anomalous transit-time dispersion in amorphous solids. Phys Rev B 12: 2455-2477. Link: https://goo.gl/1ci3i3 ; Link: https://goo.gl/JU4eSW ; Link: https://goo.gl/W5GYKy

90. Q Gu, EA Schiff, S Grebner, R Schwartz (1996) Non-Gaussian transport measurements and the Einstein relation in amorphous silicon. Phys Rev Lett 76: 3196-3199. Link: https://goo.gl/yozvjc

91. H-P Müller, R Kimmich, J Weis (1996) NMR flow velocity mapping in random percolation model objects: Evidence for a power-law dependence of the volume-averaged velocity on the probe-volume radius. Phys Rev E 54: 5278-5285; A Klemm, H-P Müller, R Kimmich (1997) NMR microscopy of pore-space backbones in rock, sponge, and sand in comparison with random percolation model objects. Phys Rev E 55: 4413-4422. Link: https://goo.gl/XpjzpJ ; Link: https://goo.gl/QM7Ti3

92. F Amblard, AC Maggs, B Yurke, AN Pargellis, S Leibler (1996) Subdiffusion and anomalous local viscoelasticity in actin networks. Phys Rev Lett 77: 4470-4473. Link: https://goo.gl/vt3Kr5

93. ER Weeks, HL Swinney (1998) Anomalous diffusion resulting from strongly asymmetric random walks. Phys Rev E 57: 4915-4920. Link: https://goo.gl/BnKsHR

94. G Zumofen, J Klafter, A Blumen (1991) Trapping aspects in enhanced diffusion. J Stat Phys 65: 991-1013. Link: https://goo.gl/YBPEDn

95. LF Richardson (1926) Atmospheric diffusion shown on a distance-neighbour graph. Proc R Soc London Ser A 110: 709-737; GK Batchelor (1950) The application of the similarity theory of turbulence to atmospheric diffusion. QJR Meteorol Soc 76: 133-146; P Tabeling, AE Hansen, J Paret (1998) in Chaos, Kinetics and Nonlinear Dynamics in Fluids and Plasmas, edited by GM Zaslavsky, S Benkadda, Springer-Verlag, Berlin. Link: https://goo.gl/7AMkR9; Link: https://goo.gl/q4Lhy7

96. BJ Alder, TE Wainwright (1957) Phase transition for a hard sphere system. J Chem Phys 27: 1208-1209. Link: https://goo.gl/SgdXma

97. DS Banks, C Fradin (2005) Anomalous diffusion of proteins due to molecular crowding. Biophysical Journal 89: 2960-2971. Link: https://goo.gl/7TVEKR

98. C Selhuber-Unkel, P Yde, K Berg-Sørensen, LB Oddershede Variety in intracellular diffusion during the cell cycle. Phys Bio 6: 025015-025024. Link: https://goo.gl/ZPjsNp

99. SC Weber, AJ Spakowitz, JA Theriot (2010) Bacterial chromosomal loci move subdiffusively through a viscoelastic cytoplasm. Phys Rev Lett 104: 238102-238106. Link: https://goo.gl/NGFAjg

100. P Schwille, U Haupts, S Maiti, WW Webb (1999) Molecular dynamics in living cells observed by fluorescence correlation spectroscopy with one-and two-photon excitation. Biophys J 77: 2251-2265. Link: https://goo.gl/VesGRS

Citation: Benhamou M, El-Moudny S (2017) Review on Pickering emulsions stabilized by adsorbed nanoparticles: Structure, Thermodynamics, Cage Effect and Subdiffusion. Int J Nanomater Nanotechnol Nanomed 3(2): 057-076. DOI: http://doi.org/10.17352/2455-3492.000022

101. M Weiss, H Hashimoto, T Nilsson (2003) Anomalous protein diffusion in living cells as seen by fluorescence correlation spectroscopy. Biophys J 84: 4043-4052. Link: https://goo.gl/jQ22jF

102. N Gal, D Weihs (2010) Experimental evidence of strong anomalous diffusion in living cells. Phys Rev E 81 020903-020907. Link: https://goo.gl/AEeZ64

103. T Dittrich, I Mora-Seró, G García-Belmonte, J Bisquert (2006) Temperature dependent normal and anomalous electron diffusion in porous TiO studied by transient surface photovoltage. Phys Rev B 73: 045407-045415. Link: https://goo.gl/iNreRk

104. ER Weeks, JC Crocker, AC Levitt, A Schofield, DA Weitz (2000) Three-dimensional direct imaging of structural relaxation near the colloidal glass transition. Science 287: 627-631. Link: https://goo.gl/yajYve

105. ER Weeks, DA Weitz (2002) Subdiffusion and the cage effect studied near the colloidal glass transition. Chem Phys 284: 361-367. Link: https://goo.gl/1YYpGb

106. ER Weeks, DA Weitz (2002) Properties of cage rearrangements observed near the colloidal glass transition. Phys Rev Lett 89: 095704-095704. Link: https://goo.gl/sN887k

107. Q Xu, L Feng, R Sha, NC Seeman, PM Chaikin (2011) Subdiffusion of a sticky particle on a surface. Phys Rev Lett 106: 228102-228106. Link: https://goo.gl/Gc7TVp

108. H Guo, G Bourret, RB Lennox, M Sutton, JL Harden, et al. (2012) Entanglement-controlled subdiffusion of nanoparticles within concentrated polymer solutions. Phys Rev Lett 109: 055901-055906. Link: https://goo.gl/GWFZEZ

109. G Marty, O Dauchot (2005) Subdiffusion and cage effect in a sheared granular material. Phys Rev Lett 94: 015701-015705. Link: https://goo.gl/DSKxyX

110. T Levy, E Sanchez-Palenca (1983) Small concentration suspension of solid particles or viscous drops in a viscous fluid. C.R.A.S. Tome 297, Série II: 193-196.

111. R Kubo, M Toda, N Hashitsume (2012) Statistical Physics II: Nonequilibrium Statistical Mechanics. Vol. 31, Springer Science & Business Media. Link: https://goo.gl/1BPG2Y

112. R Zwanzig (2001) Nonequilibrium Statistical Mechanics. Oxford University Press; also, R Zwanzig (1961) Statistical Mechanics of Irreversibility, Vol. 3 of Lectures in Theoretical Physics, Interscience, New York. Link: https://goo.gl/MCBWCa; Link: https://goo.gl/gkdeds

113. GR Kneller (2011) Generalized Kubo relations and conditions for anomalos diffusion: Physical insights from a mathematical theorem. J Chem Phys 134: 224106-224112. Link: https://goo.gl/bqH2V9

114. SG Samko, AA Kilbas, OI Marichev (1993) Fractional Integrals and Derivatives, Theory and Applications, Gordon and Breach Science Publishers.

115. IS Gradshteyn, IM Ryzhik (1980) Tables of Integrals, Series and Products. Academic New York. Link: https://goo.gl/Vs7Qzr

116. MP Allen, DJ Tildesley (1989) Computer Simulation of Liquids. Oxford university Press. Link: https://goo.gl/PQ31gG

117. HJ Berendsen, JPM Postma, WF van Gunsteren, ARHJ DiNola, JR Haak (1984) Molecular dynamics with coupling to an external bath. J Chem Phys 81: 3684-3690. Link: https://goo.gl/JpsQJE

118. BVR Tata, AK Sood, R Kesavamoorthy (1990) Structure factor of charged colloidal suspensions using Brownian-dynamics simulation: comparison of Yukawa and Sogami pair potentials. Pramana-J Phys 34: 23-31. Link: https://goo.gl/vwJZta

119. GS Chirikjian, AB Kyatkin (2000) Engineering applications of noncommutative harmonic analysis: with emphasis on rotation and motion groups, CRC Press, p.23. Link: https://goo.gl/zcX5yr.

Citation: Benhamou M, El-Moudny S (2017) Review on Pickering emulsions stabilized by adsorbed nanoparticles: Structure, Thermodynamics, Cage Effect and Subdiffusion. Int J Nanomater Nanotechnol Nanomed 3(2): 057-076. DOI: http://doi.org/10.17352/2455-3492.000022